University of Tabriz

Faculty of Civil Engineering

Department of Water Engineering

Thesis is approved for the degree of Master of Sciences in Civil Engineering

Title

Numerical and Experimental Study of Flow in Open Channels with Cylindrical Roughness

Supervisor

Dr. Yousef Hasanzadeh

Adviser

Dr. Akram Abbaspour

Researcher

Soheil Zehsaz

January 2016

Surname: Zehsaz	**Name:** Soheil
Thesis title: Numerical and Experimental Study of Flow in Open Channels with Cylindrical Roughness	
Supervisor: Dr. Yousef Hasanzadeh **Advisor:** Dr. Akram Abbaspour	
Degree: Master of science **Fileld:** Water Engineering **Faculty:** Civil Engineering	**Major:** Civil Engineering **University:** University of Tabriz **Graduation date:** January 2016 **Page:** 93
Keywords: Roughness function ΔU^+, Cylindrical rib Roughness, Turbulence, Velocity profile	

Abstract

In this study effect of the different types of surface roughness on a turbulent boundary layer was studied using 1D velocity measurements in a relatively high Reynolds free-Surface water channel. The roughness consisted cylindrical ribs with several P/D (P is the roughness spacing, D is the roughness height). The roughness elements were aligned in a direction transverse to the flow. The experiments involve one-dimensional flow velocity, water surface profiles and bed pressures and forces with different Reynolds numbers. A series of 12 tests of fully rough turbulent subcritical flow over two dimensional transverse repeated cylindrical ribs was undertaken in which the ribs were varied to give uniform rib spacing-to-height ratios of P/D = 5-20. The results show that the normalized velocity U^+ for all the surfaces has significantly decreased comparing to smooth bed. The average values of the drag C_f and friction Ft coefficients are reduced with increasing of roughness distances on rough beds, also the amount of the drag and friction coefficients are the highest values on the cylindrical roughness with P/D= 15, H= 8 cm, D= 6 mm. Flow development in an open-channel with rough beds was investigated using FLUENT. The RNG k-ε turbulence model was used for subcritical flow cases. The volume of fluid (VOF) method was used to allow the free-surface to deform freely with the underlying turbulence. The main purpose of this study is to examine the effects of surface roughness on a turbulent boundary layer in a relatively different Reynolds numbers. The determination of velocity profile in turbulent open channels with rough bed is a difficult task due to the significant effects of the roughness. The velocity distributions in the log-region for the rough wall were determined and the roughness function ΔU^+, was evaluated compared to the smooth bed. The results show that the mean profiles of all the surfaces collapse well in the velocity defect form.

Contents

Types of rough substrates

roughness of type d

roughness of type k

Intermediate roughness

Numerical Examination of Flow on Rough Beds

Chapter three: Methods

Laboratory Investigation of Flow on a Rough Bed

Laboratory Equipment

Flume

Model of rough bedding

Means of current measurement

Depth Finder

Speedometer

Measuring tool during roughness

Test Method

Dimensional Analysis

Numerical simulation of flow on rough bed

Network Range Flow

Finite Volume Method

Selecting the Computational Method

Basic Equations of Turbulence and Flow Phases

Definition of Boundary and Primary Flow Conditions

Definition of physical properties of materials and operating pressure

Initial guess of flow field

Performing Flow Calculations

Model Operating Process

Creating Input and Output File

Adaptation and Optimization

Generating images and charts and reporting on the solution

Turbulent flow structure

List of shapes and tables

List of symptoms

B=logarithmic profile additive constant;

C_f= wall skin friction coefficient

D=roughness height;

D^+=roughness Reynolds number, $D^+=Du_*/\nu$;

Fr_1=Froude number, $Fr_1=u_m/(gH)^{0.5}$;

F_t=friction factor, $F_t=8[u_*/U_1]^2$;

g=gravitational acceleration;

H=upstream mean flow depth;

p=crest-to-crest spacing;

R=hydraulic radius, $R=(bH)/(b+2H)$;

Re=Reynolds number, $Re=4Ru_m/\nu$;

S_w=water surface slope;

u_m =mean velocity;

u_*=shear velocity, $u_*=(gRS_w)^{0.5}$;

y^+=the normalized effective height, $y^+ = \frac{u_* z}{\nu}$;

z=elevation above the between-rib cavity base;

zc= rib crest elevation;

κ=von Karman's constant, κ=0.4–0.42;

ν= fluid kinematic viscosity,

τ =wall shear stress

First Chapter

General

Introduction

The importance of using open channels in river engineering such as water transfer systems is well known. The hydrodynamic structure of these types of currents, which are often turbulent, is also important. There has been a great deal of research on this topic by researchers, including laboratory studies and numerical analysis. Also, the study of flow hydrodynamics in open channels in the presence of barriers with different shapes has attracted the attention of researchers, in which case numerical and laboratory work has been done.

Hydraulics is known as one of the branches of fluid mechanics in which, unlike the branch of hydrodynamics, hydraulic is widely used in experimental and laboratory aspects.

The necessity of using experimental and laboratory results is due to the complexity of the influence of various natural and abnormal factors on the mechanical behavior of water.

Among the various methods of water transfer, the use of gravity force and the movement of water in a free-surface flow, along with the creation of associated hydraulic channels and structures such as overflows, valves, etc. are the most common methods. It is in irrigation and water supply that it requires engineers and specialists to understand the laws governing such streams as open-channel hydraulics. In open-channel hydraulics, while explaining the principles and rules governing free flows and their applications, as well as investigating the gradual and spatial variable currents in waterways, the hydraulic principles governing facilities such as valves and overflows, as control structures. Current flow, hydraulic design of structures such as transformers, bridges and ditches, as well as flood control and wave propagation in canals and rivers are discussed.

In this study, water surface profiles and longitudinal flow velocities on coarse-grained cylindrical substrates, with k height and p-wavelength in different dimensions, are investigated and investigated. Investigation of surface water profiles and velocity profiles as a function of geometrical and hydraulic parameters determined by experimental flow tests on the physical model is possible. Two-dimensional turbulence models are used to simulate the turbulent flow on rough beds and the free flow surface is determined by numerical method except fluid volume. The influence of the rough bed on the turbulent flow structure is investigated by calculating the water surface position, velocity profile and shear stress of the bed in this model. Laboratory data are used to evaluate the numerical model.

Necessity of research

In open channels, including canals and rivers, the flow is quite turbulent. Investigation of the impact of roughness on flow structure in hydraulic issues is important and is used to predict flow turbulence. On the other hand, the results obtained from laboratory investigations are also used for the validation and analysis of numerical methods. Studies show that the combination of physical and numerical models is effective in the context of turbulent currents and improves the accuracy of the results.

Second chapter

Literature review

Introduction

In open channels such as rivers, the flow is quite turbulent. Investigation of the impact of roughness on flow structure in hydraulic issues is important and is used to predict flow turbulence. On the other hand, the results obtained from laboratory investigations are also used for the validation and analysis of numerical methods. Studies show that the combination of physical and numerical models is effective in the context of turbulent flows and enhances the accuracy of the results.

In turbulent flows there is a close relationship between flow resistance, turbulence and sediment transport, and there have been many studies in this area over the last four decades. In flat substrates, considering the balance between turbulence generation and energy dissipation rate, two internal and external flow zones are created as shown in Fig. 1-2. The underlying layer is important in this type of flow and is divided into two substrates, including the viscose substrate (linear substrate and buffer substrate) and the superstructure (logarithmic region) (Fig. 2-1). In the free water area, the amount of energy loss is greater than the energy production because the intensity of vertical turbulence is strongly influenced by the water level. In the middle region the energy balance is maintained and the surface area of the outer region of the flow is turbulent and the viscosity effect is negligible.

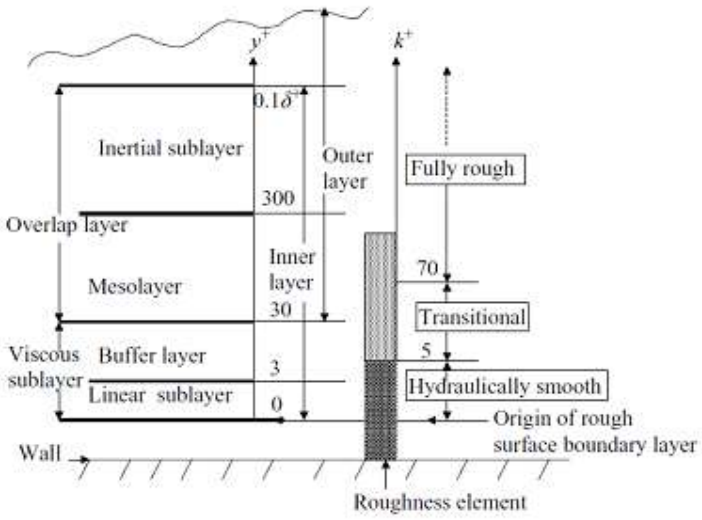

Figure 2-1- Different layers of flow in turbulent flows (Jimens, 2004)

In the rough walls, the roughness elements affect the flow structure and, as a result, the flow structure with the smooth bed is very different. According to Jimens (2004), the most influence of roughness on velocity and resistance coefficient profiles is near bed bottom. The velocity profiles are divided into three areas (wall, inner, and outer) according to the height of the roughness (Figure 2-2). The universal logarithmic law of velocity is established in accordance with Figure (2) and is added to the equation to illustrate the effect of roughness on the velocity equation of the parameter of the roughness function. The roughness function parameter is defined as a function of the dimensionless roughness. The effect of wall roughness is divided into three parts. Hydraulically smooth in the $y^+ < 5$ bed area, $5 \le y^+ \le 70$ is the intermediate-bed rough and $y^+ > 100$ -bed is rough. In addition, Byron et al. (2004) showed that it is necessary to determine the shear velocity parameter in coarse-grained turbulent currents. This parameter is also used to estimate the flow resistance as a surface friction parameter C_f.

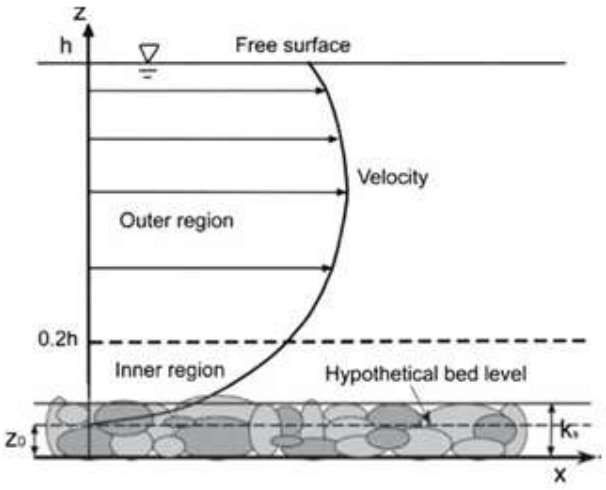

Figure 2-2: Logarithmic velocity profile on rough bed (Jimens, 2004)

The turbulent flow on the rough walls was studied by researchers such as Hagen in 1854 and Darcy in 1857 and the pressure drop was studied at various points. The theory of turbulent flows gradually developed. The pressure drop in the pipes in the turbulent currents was independent of the flow viscosity force while being influenced by the roughness of the flow walls. This was the source of the beginning of the theory of boundary layer relaxation. The flow on smooth beds does not become completely turbulent and the boundary layer theory becomes more complex (Byron et al., 2004).

The flow on the wall is influenced by two factors: the length scale of the wall distance and the fluid viscosity. Near the wall of fluid viscosity ν are important and shear velocities are $u_\tau = (\tau / \rho)^{1/2}$. In this respect, τ is the shear stress of the current and ρ is the fluid density. Flow theory near the wall based on the momentum equation shows that Reynolds stresses are proportional to $u_\tau^{\,2}$ in the boundary layer and the shear velocity u_τ is the velocity index.

The effect of fluid viscosity on $y^+ \approx 5$ and in the active region of $10 \le y^+ \le 100$ current is very important. In this area, turbulent currents and energy losses occur.

At the upper wall distances, the thickness of the boundary layer d is determined at different distances of the structure. The shear Reynolds number is the measure of the separation of the outer and inner lengths of the boundary layer. If the thickness of the boundary layer d is large enough, the outer layer and the buffer layer overlap and y is large enough that the fluid viscosity does not affect. In such circumstances, the longitudinal scale is only the distance from the wall. The average longitudinal velocity as a logarithmic distribution is obtained from the following relation:

$$U^+(y) = k^{-1} \log y^+ + A \qquad (2\text{-}1)$$

In this respect, the Karman coefficient is $k \approx 0.4$ and depends on the properties of the layer. A is the coefficient constant on non-slip boundaries. Since the relation (2-1) for 1 << y^+ is established, the values of the coefficient A depend on the viscous layer. For smooth walls, the experimental coefficient is $A \approx 5.1$.

The equation of velocity profile under 50 <y is as follows:

$$U^+(y) = k^{-1} \log y^+ + A + \Delta U^+ \pi_{k^{-1}} W(y/\delta) \qquad (2\text{-}2)$$

In this respect W represents the dynamic effect of the outer layer and can be ignored for $y/\delta < 0.15$. The function W for 1 is twice that of (w(1) = 2).

If the height of the coarse elements is large, the viscous buffering layer is affected which will change under the conditions of k^+<100-50 constant coefficient A because the logarithmic layer produces the highest turbulent energy. Also, if k is neglected compared to the thickness of boundary layer δ, the roughness of the bed affects the nature of the flow. According to the logarithmic form of Equation (2-2), the frictional velocity is less dependent on δ. In near-wall currents with a low pressure gradient of $U_\delta / u_\tau \approx$20-30 degrees the viscosity length depends on the flow rate and the fluid viscosity and is independent of the Froude number. In industrial processes with a water velocity of U_δ =1-10 m / s the viscose length scale is 2 to 20 μm.

The roughness has the greatest effect on the velocity profiles near the walls and therefore the friction coefficient. Preliminary studies on rough substrates were carried out by Nikoradze (1993) in rough tubes using fine sand. The results of these studies showed that the logarithmic velocity distribution is close to the walls, and the Karman constant coefficient in the rough bed is equal and the velocity profile is as follows.

$$U^+(y) = k^{-1} \log(y / k_s) + 8.5 + \pi_{k^{-1}} W(y/\delta) \qquad (2\text{-}3)$$

In the above relation, k_s indicates roughness equivalent to sand. Taking into account the position of measurement, Rupach et al. (1991) presented the following equation:

$$U^+(y) = k^{-1}\log y^+ + 5.1 + \pi_{k^{-1}} W(y/\delta) - \Delta U^+ \quad (2\text{-}4)$$

In which the first three sentences are related to the flat bed and the last sentence shows the effect of bed bumps or bumps or roughness on the flow rate. The velocity profiles with another relation are determined as follows:

$$U^+(y) = k^{-1}\log(y/k_0) + \pi_{k^{-1}} W(y/\delta) \quad (2\text{-}5)$$

In this respect k_s, $k_0 = 0.033$ is roughness length.

As the surface drag coefficient differs in the boundary layer on the rough bed. The flow velocity U at the depth of y under smooth and rough bed conditions of Equation (2-4) can be written as follows:

$$U_r^+ + k^{-1}\log U_r^+ = k^{-1}\log(R/k_s^+) + 8.5 = B_r$$

$$U_l^+ + k^{-1}\log U_l^+ = k^{-1}\log Ry + 5.1 = B_l \quad (2\text{-}6)$$

Where $R = Uy/\nu$ is the Reynolds number of currents, $U^+ = U/u_\tau$ and the indices l and r belong to the smooth and rough bed. The above two equations are similar to each other and U^+ also increases the function B uniformly. The difference in drag force between the smooth and rough bed is determined as follows:

$$k^{-1}\log k_s^+ - 3.4 = B_l - B_r \quad (2\text{-}7)$$

For $k_s^+ = k_s u_\tau/\nu < 4$, the surface resistance in the bed is less than that of the flat bed, which is unknown. Coarse elements provide significantly higher surface resistance than flat substrates due to higher turbulence energy production in coarse substrates. Therefore, in many cases $k_s^+ \approx 4$ is the low roughness limit where the flow resistance in the rough and rough substrates is the same. In some cases, rough surfaces reduce the drag force. For example, the flow on narrow grooves along the water flow can be named. Studies show that grooves reduce drag resistance by up to 10% (Nezoo et al., 1997).

Under $B_l >> B_r$, the surface viscosity coefficient of the fluid viscosity is negligible compared to the surface roughness coefficient and the flow is independent of the fluid viscosity. In such circumstances it can be concluded that:

$$\frac{u_{\tau,r}}{u_{t,l}} \approx \frac{B_l}{B_r} \quad (2\text{-}8)$$

In the flat bed B_l in the logarithmic layer is approximately 20-30. Therefore, under $B_r < B_l/\sqrt{2}$, the surface resistance is more than twice that of the smooth surface. Then $B_l - B_r \geq 7.5$ and $k_s^+ \geq 80$ are set.

2-2- Laboratory study of flow on rough substrates

2.2.2 Types of rough substrates

2.2-1-1- roughness type d

The difference between the two substrates k and d was expressed by Perry et al. (1969) (Figure 2-3). This type of roughness is in the form of narrow grooves along the flow. In type d roughness the effective roughness k_s is not proportional to the height of the roughness k and is proportional to the thickness of the boundary layer by $k_s \approx 0.02$. This is not the case for the boundary layer with negative pressure gradients. In such conditions, k_s is proportional to the boundary layer Δy relative to the top of the protuberance and is independent of the length of the grooves.

2.2-1.2- roughness of type k

In roughness type k the effective roughness k_s is proportional to the height of the roughness k. The ratio k_s/k in this type of roughness depends on the geometric properties of the roughness k and the roughness density λ (the ratio of the area of the forehead to the area of the roughness wall).

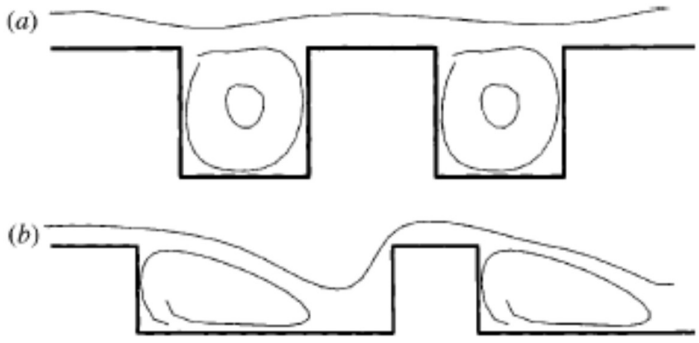

Fig. 2–3 Comparison of the substrate (a type d and b) type k (Perry et al., 1969).

Simson (1973) investigated the effect of dimensionless parameter on drag coefficient on roughness k-type surfaces and proposed the following relation:

$$\Delta_0 U^+ \approx \Delta U^+ - 25k/\delta \quad (2\text{-}9)$$

Where $\Delta_0 U^+$ for $k/\delta = 0$ is the ideal value of the dimensionless velocity ($\Delta_0 U^+ \approx \Delta U^+$).

Studies show that if the groove width is p greater than 3-4 times the roughness height k, the roughness is k-type.

2.2.1.3 Intermediate roughness

If the flow regime is such that k^+ is not large enough and the flow is completely coarse-grained, the flow regime becomes unclear, which is called intermediate or transient conditions.

The results of Stowser and Rudy's (2004) research showed that in roughnesses d the shape of the roughness bands is close and therefore the vortices are created between the holes and can be ignored outside the holes.

(2000) investigated kinetic energy and shear stresses in rectangular rough substrates. The results showed that the kinetic energy and shear stress due to turbulence inside the cavities were small and reached a maximum value at a little distance above roughness. In coarse-grained substrates with greater k-spacing, most eddy currents occur at the foot of the roughness before the next roughness.

Brents and Madsen (2000) conducted a study of triangular roughness beds and concluded that vortices formed with a longitudinal scale of roughness height started from roughness and continued to the boundary layer.

(2001) investigated the turbulent flow structure in rectangular and circular rough substrates for the upper Reynolds number range. In this study, two-dimensional velocity profiles were measured with laser speedometers. The results showed that the velocity profiles are logarithmic and the velocity component ΔU^+ in the velocity equation for the circular substrates (p / k =4) is higher than the square substrate (p / k =2) and is more smooth than both substrates. No. Also Reynolds stresses in circular substrates are larger than square and flat substrates. The velocity component corresponding to ΔU^+ roughness for the smooth, square, and circular substrate was set to zero, 4.1, and 13.5, respectively (Fig. 2-4).

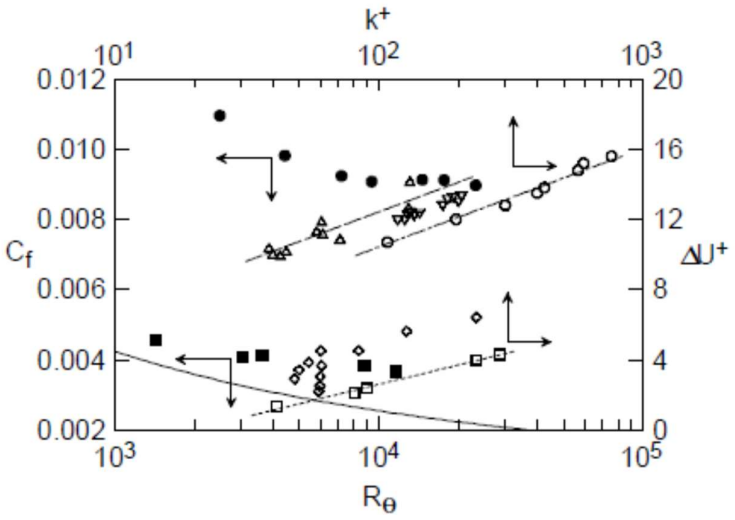

Figure 2-4: Variations of d values for dimensionless roughness k^+ and drag coefficient C_f for boundary layer adrenoids (Bisquila et al., 2001).

Nikora et al (2004) examined the velocity profile on the roughness and concluded that the shape of the velocity profile depends on several factors such as the geometry and dimensions of the roughness and flow conditions and can be presented in linear, logarithmic, power, or velocity forms. Be a combination.

Coleman et al. (2006) investigated velocity profiles on wavy sandy roughnesses. The results showed that the velocity profiles are logarithmic in the near roughnesses with p / k <10 (distance to height ratio) ratio, while p / k> 10.

Coleman et al (2007) studied turbulent currents on a square bed. In this study, the relative roughness distances were in the range of 16-1 p / k and the relative submergence was 0.9 k / H (H = water depth). Laboratory studies include measurements of velocity vectors, water surface profiles, bed pressure and shear forces. The maximum drag forces correspond to roughness p = 8/k (Figures 2-5 and 2-6).

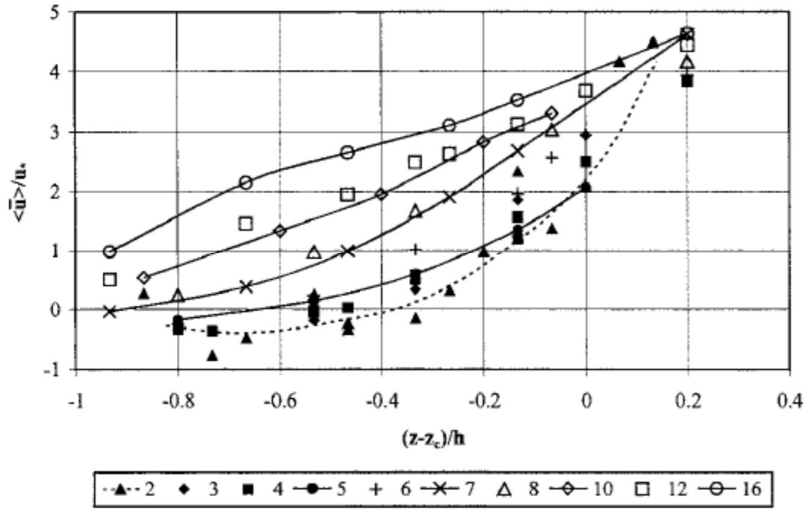

Figure 2-5 - Speed profiles in square roughness for different p / k values (Coleman et al., 2007)

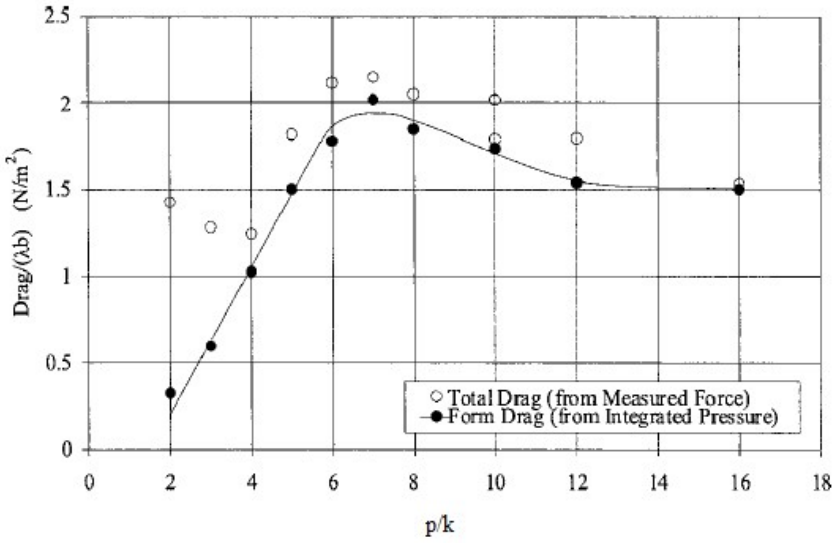

Figure 2-6- Drag force variations for different p / k values (Coleman et al., 2007)

Nikora et al. (2007 a, b) presented dual average hydrodynamic equations (in time and space) on rough substrates. According to these studies, four types of flows for partial drowning can be considered. In Type (I) flow the relative submergence is high and the outer layer is logarithmic at the top and the bottom layer is created at the bottom of the logarithmic layer and above the roughness crown and the mean temporal flow is affected by the roughness elements.

Stosser and Nikoradze (2008) examined turbulence properties in open channels with a rough squared bed. In this study, the roughness of type k (p / k= 9) and transient type (p / k= 4.5) and the type of submergence were moderate (H/ k = 6.5). According to Figures (2-7) and (2-8), the laboratory data are in good agreement with the LES model. Also shown in Figure (2-9), the simulation results of LES model for bed shear stress values were performed using HYDRO3D software.

The shear stress distribution of rough walls for two types of roughness is shown in Fig. (2-9). The critical points of stress are near the rough wall. Also, shear stress at the top of the roughness (p / k = 9) is negative indicating the rotation of the flow in this area, and for the transient type roughness (p / k = 4.5) there is also a negative tension between the square roughnesses.

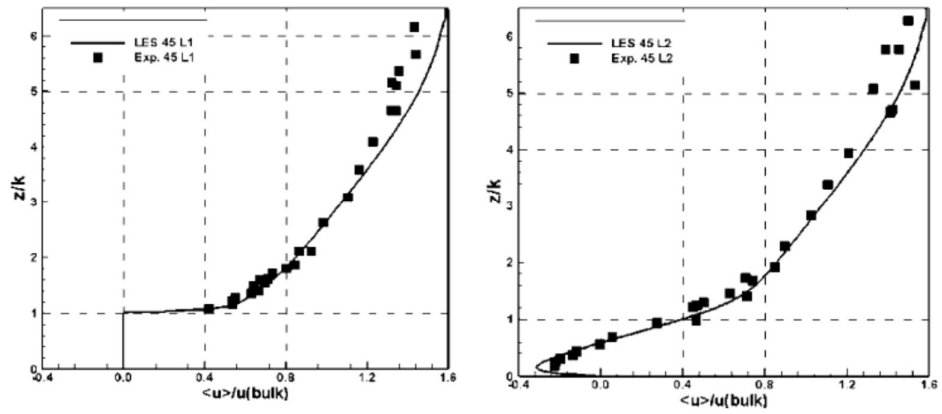

Figure 2.7 Comparison of the vertical velocity distribution obtained from the LES model and the experimental data on the right and left walls for relative roughness distances of p / k =4.5 (Stoser & Nikoradze, 2008).

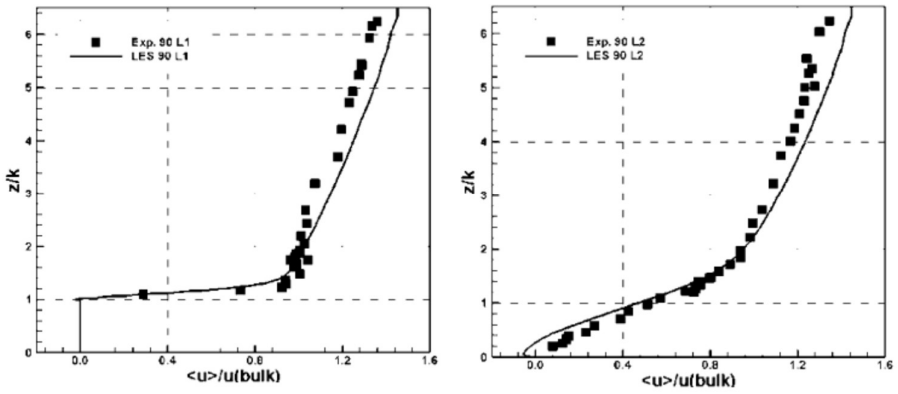

Figure 2.8- Comparison of the vertical velocity distribution obtained from the LES model and the left and right wall laboratory data for relative roughness distances of p / k =9 (Stoser & Nikoradze, 2008).

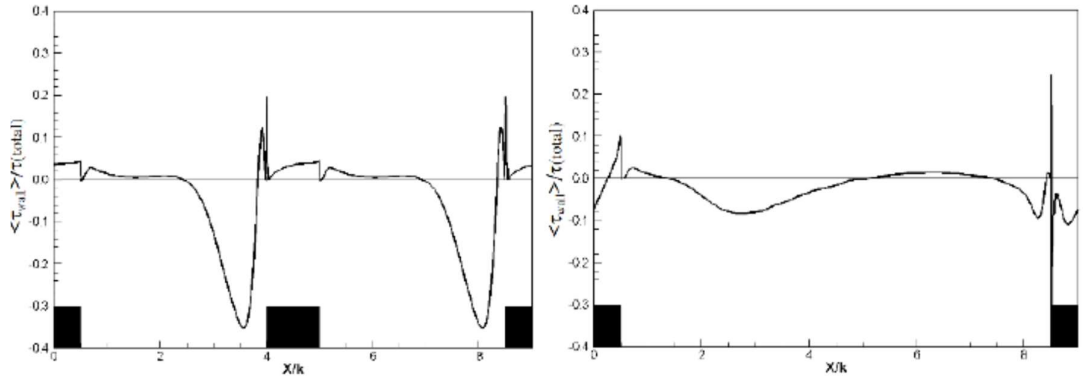

Fig 2. 9- Medium shear stress simulated by LES model on substrate with conditions p / k =4.5 and p / k =9 (Stoser & Nikoradze, 2008)

Go and Julien (2008) developed the application of velocity logarithmic law in open channels. The velocity profile in the open ducts consists of three components, the first component consisting of the wall law and is determined by considering the constant stress. The second component is the effect of eddy current, bed roughness and gravitational force, and the third component is maximum velocity. The revised logarithmic velocity law is in good agreement with the laboratory data of Coleman (1986) and Lynn (1986) (quoted by Go and Julien, 2008) (Figs. 10-10).

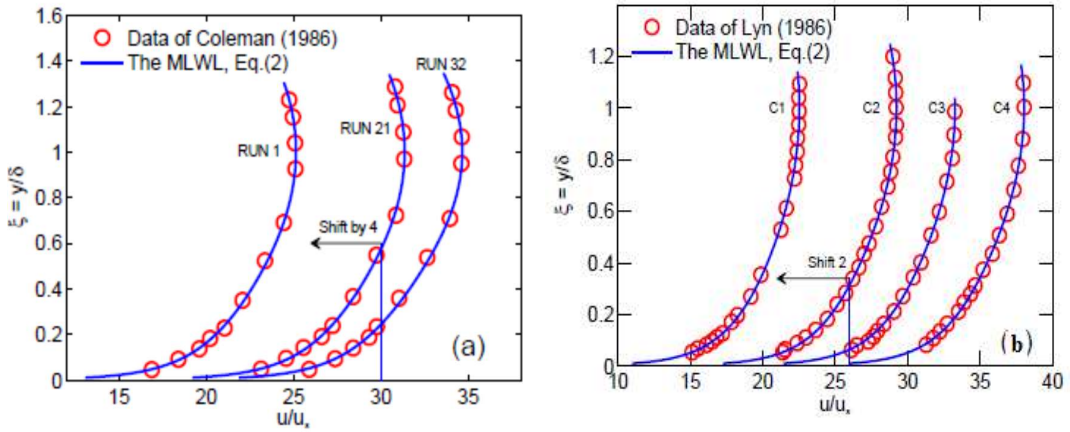

Figure 2.10 - Comparison of the Modified Logarithmic Law of Speed of Laboratory Data a) Coleman (1986) b) Lynn (1986) (Go and Julien, 2008)

Benakardi et al (2008) examined velocity profiles during coarse-bed turbulent flow. The results showed that the maximum velocity was below free water level, which is called dip phenomenon. In this research, the velocity distribution in the outer layer of the flow is evaluated based on Navier-Stokes equation analysis. The proposed speed distribution law in this scheme

includes an additional C_{Ar} parameter that depends on the position of the maximum speed. The results obtained from the proposed model and the laboratory data are in good agreement. The proposed relationship of Benakardi et al. (2008) is as follows.

$$\frac{U(\zeta)}{u_*} = \left(\frac{\zeta_i^2 + \zeta_i + C_{Ar}}{\zeta^2 + \zeta + C_{Ar}}\right)\left[\left(\frac{(\zeta^2/4 + \zeta + C_{Ar} Ln(\zeta)) - (\zeta_i^2/4 + \zeta_i + C_{Ar} Ln(\zeta_i))}{\zeta_i^2/2 + \zeta_i + C_{Ar}}\right) \times \frac{\alpha}{k} + \frac{1}{k} Ln\left(\frac{0.2h}{k_s}\right) + B_s)\right] \quad (2\text{-}10)$$

In this respect $\zeta = z / h$ is the relative distance from the floor, ζi is the maximum velocity position, and C_{Ar} is the constant coefficient of the equation. Figures (2-11) and (2-12) illustrate the evaluation of the above formula with the data of Nezou et al. (1997) and this method by the logarithmic distribution of velocity and the Koles's law (1956) (Benaccardi et al., 2008). It has also been compared.

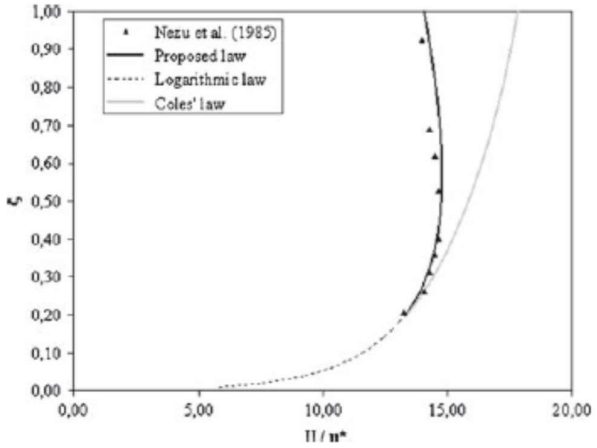

Figure 2-11- Validation of the Proposed Formula in a Rectangular Channel for U = 0.29 m / s (Benaccardi et al., 2008)

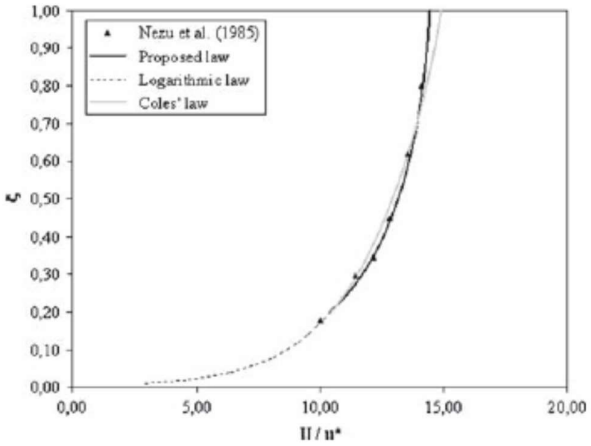

Figure 2.12- Validation of the Proposed Relationship in a Rectangular Canal for U = 0.37 m / s (Benakdari et al., 2008)

Volino et al (2007) investigated the turbulent currents on a square rough bed and compared them with the results of a study on rough beds on a wire mesh and a flat bed. The average flow velocity profiles are shown in Fig. 13-2. The results showed that flow roughness is effective on velocity profiles and decreases in square roughness of dimensional velocity profiles.

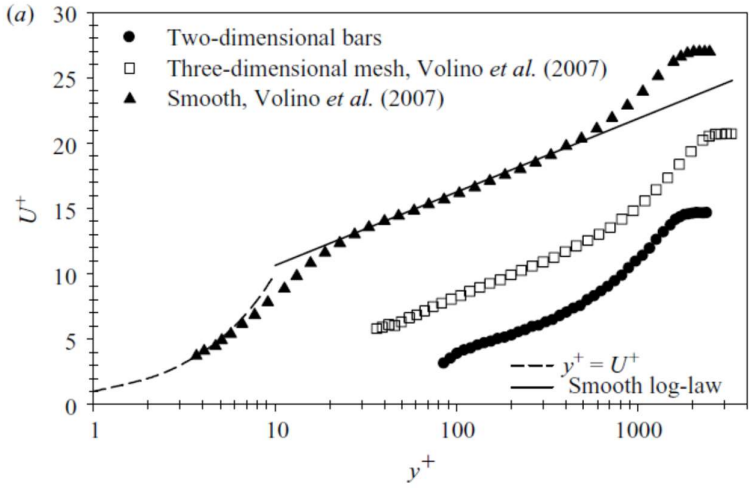

Figure 2-13 - Comparison of the average velocity profiles in rough and smooth bands (Volino et al., 2007)

Numerical investigation of flow on rough substrates

Leonardi et al (2003) simulated turbulent flows on a square bed using a direct numerical simulation (DNS) method. In this study, a wide range of roughness intervals of $7 \leq p/k$ was investigated and the results showed that vortices occur immediately before and after rotation. The maximum drag force occurs for the relative roughness distance of p/k =7.

Ashrafian et al. (2004) simulated the flow over rough rough surfaces using DNS method. In this study, the Reynolds shear number was $Re_{\tau=}$ 400, which is a coarse-grained transient flow and the ratio of roughness-to-height ratio was p/k = 8. Figure (2-14) shows the simulated flow lines with the numerical DNS model.

In the figure (2-15), the dimensional velocity profile compared to the flat bed shows that the ΔU^+ value is approximately 8.3 according to the results of this study.

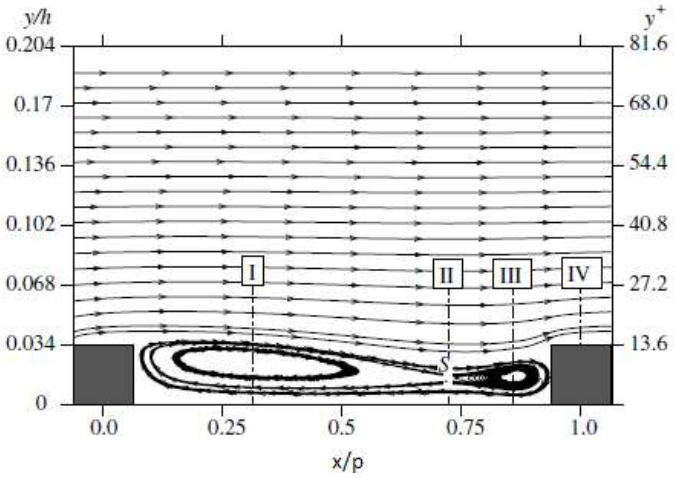

Figure 2-14- Display of Simulated Flow Lines on a Rough Square Bed (Ashrafian et al., 2004)

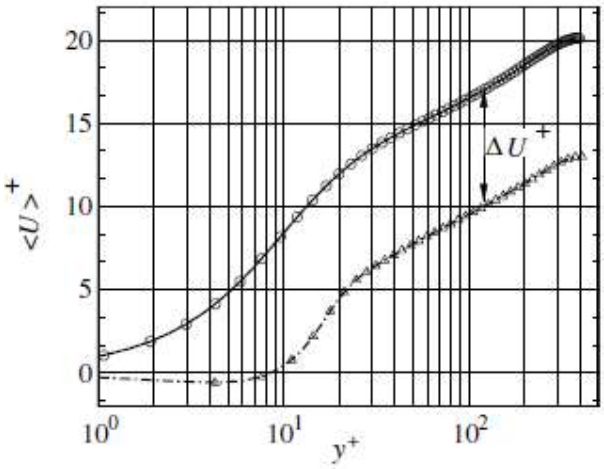

Figure 2-15- Simulated velocity profile using DNS numerical method (Ashrafian et al., 2004)

Lee et al. (2009) studied turbulent flows on square rough substrates. In this study, we simulate direct numerical simulation (DNS), turbulent boundary layer, Reynolds stresses, and drag forces. The roughness height of the boundary layer thickness was $k/\delta = 0.05$. Investigations showed that the kinetic energy distribution is similar to that of the flat substrates and the influence of roughness on the velocity distribution in the outer layer is evident. The longitudinal mean velocity distribution follows the logarithmic law, and the laboratory data show good agreement with the numerical model. The value of deceleration of velocity values according to Figure (2-16) is 9.86. Studies also show that in rough substrates the velocity in the outer layer is similar to that of the flat substrate but in the inner layer the velocities are affected by roughness and the velocities decrease. The eddy structure and instantaneous velocity vectors of one of the roughnesses are shown in Fig. 17-2.

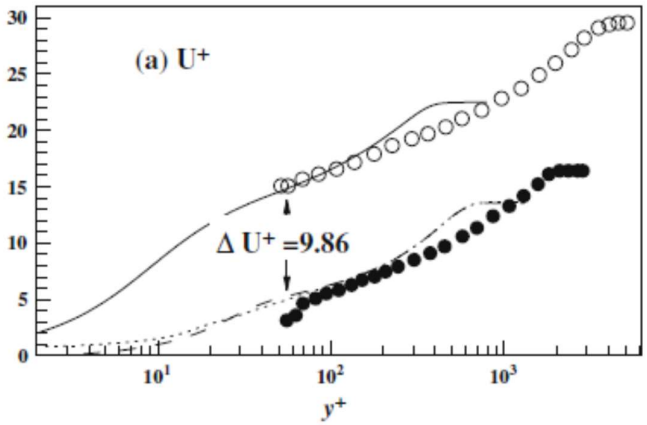

Figure 2-16 - Simulated velocity profiles using the numerical DNS method (Lee et al. 2009)

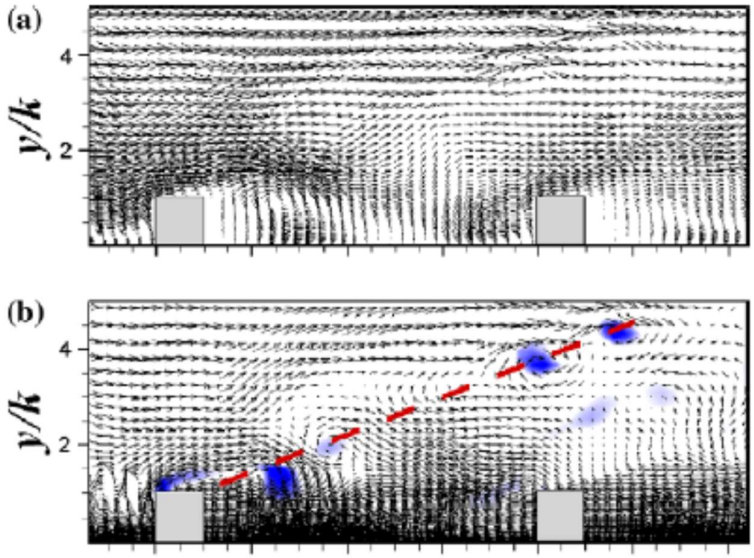

Figure 2-17- Numerical representation of a) eddy structure b) field velocity vector fields near roughness (Lee et al. 2009)

In another study, Lee et al. (2011) examined the effect of cubic roughness bed on bubbling currents. In this study, direct numerical method (DNS) was used to simulate the boundary layer of turbulent currents and Reynolds stresses. The roughness intervals along the longitudinal channel were considered as p/k = 2 and p/k =8 ratios and the results of this study were compared with the results of continuous square cube roughness. Surveys showed that the decline was in the range of 6.7 to 7 (Figure 18.2). Also, the changes of drag coefficient C_f and shear velocity at non-dimensional intervals x/θ_{in} in (θ_{in}, thickness of momentum) for rough substrates are

shown in Fig. 19-2. The variation of Reynolds stress distribution at different roughness intervals is shown in Fig. (2-20).

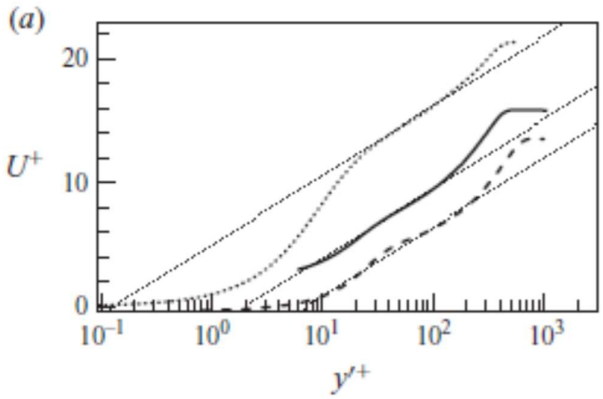

Figure 18-18 - Comparison of dimensional velocity profiles in the cubic and smooth rough bed (Lee et al., 2011)

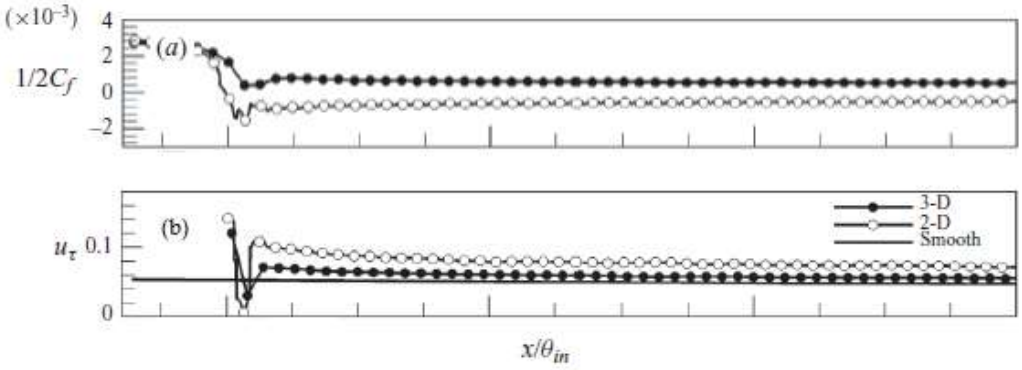

Figure 2-19- Spatial Variations (a) Drag Force Coefficient (b) Longitudinal Shear Speed Compared to Flat Bed (Lee et al., 2011)

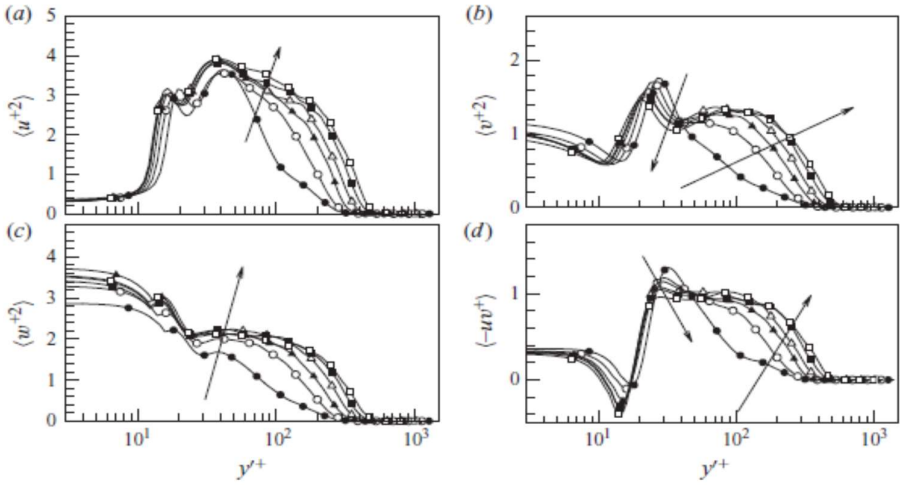

Figure 2-20- Variations of dimensional Reynolds stresses at different longitudinal distances on the rough cube bed (Lee et al., 2011)

Third Chapter
Materials and Methods

3.1. Laboratory study of flow on rough bed

3.1.1 Laboratory equipment

3-1-1-1- Flume

In this study, the open channel in the Fluid Mechanics Laboratory of the Department of Mechanical Engineering of the University of Tabriz with a rectangular cross section of 20 cm width and 40 cm height will be used. The walls of the canal are glass and as a result water surface profiles and flow conditions are visible. Figure (2-3) shows the experimental platform plan.

3-1-1-2- Model of rough bedding

The cylindrical rough substrates are made of metal, with heights of 6 and 10 mm in accordance with Figure (1-3). The bed width is equivalent to the rectangular channel width of 0.20 m. Roughnesses were mounted at the bottom of the canal in accordance with Table 3-1. Complete sealing was performed between the floor of the canal and the roughness on it so that there was no flow between the floor and the roughness. Roughness intervals vary, with a relative P / D interval of 5 to 15 for roughnesses of 10 mm and 10 to 20 for roughnesses of 6 mm. The physical and hydraulic properties of the flow in the laboratory tests are presented in Table (1-3). In this table are $Fr_1=u_m/(gH^{0.5})$ and $Re= 4Ru_m/\nu$ where H is the water depth upstream of the channel, R is the hydraulic radius, u_m is the average flow rate and ν is the kinematic viscosity of the water. From the relationship $u_*=(gRS_w)^{0.5}$ (S_w the slope of the surface of the water) is obtained, in all tests the flow is roughly turbulent and the condition $y^+=ku_*/\nu>70$ is established.

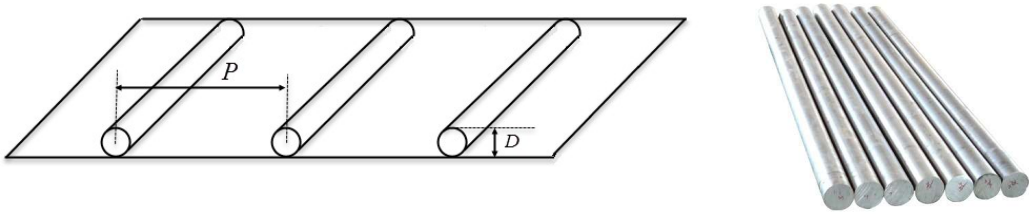

Fig. 3-1- Displays a rough cylindrical bed

3.1.1.3 Means of current measurement

3-1-1-3-1- Point gauge

To measure water depth and water level at different intervals of rough bed, a point gauge of 0.1mm was used. In the water level profiles, the initial roughness is 4.5 cm upstream of the first roughness (x = 0).

3-1-1-3-2- Velocity gauge

A Micro Propller Velocity Meter was used to measure velocity profiles. The mechanism of operation of this speedometer is based on the impedance changes due to the probe period. Accuracy measurement accuracy is 0.1 cm / s and speed measurement range is 5 to 200 cm / s.

3-1-1-4- Scale measuring during roughness

To measure the velocity at different distances of the rough bed, a strip was installed on the wall of the flume so that it was zero at the beginning of the rough bed and the speedometer was placed at different distances.

Table 3.1 Physical and Hydraulic Properties of the Laboratory Model

Beds	**P/D**	**H (cm)**	**D (mm)**	**u_m (cm/s)**	**Re**	**Fr_1**	**u_* (cm/s)**	**S_W $\times 10^3$**

	5	8	10	20.6	38160	0.24	4.71	4.9
	10	8	10	19.03	35251	0.22	3.63	2.9
	15	8	10	20.3	37604	0.23	3.23	2.3
Cylindrical (1)	5	6	10	14	21728	0.19	6.93	12.6
	10	6	10	18.9	29333	0.25	6.44	10.9
	15	6	10	19.54	30326	0.25	5.12	6.9
	10	8	6	15	27786	0.18	5.60	6.9
	15	8	6	16.47	30509	0.19	8.36	15.4
	20	8	6	20.1	37233	0.23	8.44	15.7
Cylindrical (2)	10	6	6	16.86	26167	0.22	7.29	14
	15	6	6	14.73	22861	0.20	6.35	10.6
	20	6	6	16.66	25856	0.22	4.97	6.5

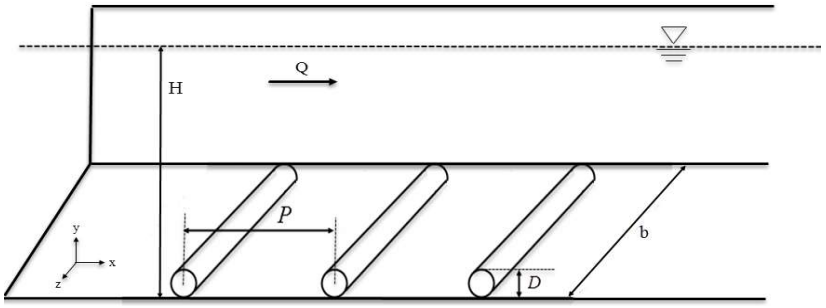

Figure 3.2 - Schematic image of the laboratory flume

Figure 3.3 - A representation of the flow on the rough bed

3.2.2 Test Method

Experimental flow experiments were performed on the rough bed as follows.

Experiments were carried out in the Flume Fluid Mechanics Laboratory of the University of Tabriz, department of Mechanical Engineering.

The flow is upstream of the subcritical flume. Subcritical flow and initial H depth were created on rough and unbroken substrates.

In each experiment, with the assurance of stable flow establishment, the surface profiles along the rough bed were measured with a 0.1 mm point gauge at different distances. In all tests, longitudinal distances were recorded using a flume glass wall strip.

For different tests of velocity profiles at different sections were measured using a micro blade speedometer. The speed range was zero to 2 m/s. Hydraulic flow characteristics with different initial Fr_1 Froude numbers were generated on rough beds and velocity and water level profiles were measured for 12 tests. The geometrical and hydraulic specifications are part of the tests presented in Table 3-1.

Figure (3-3) shows a demonstration of the flow on the rough bed. The results of the experiments and the experimental evaluation of the flow are presented in the next chapter.

3.2.2 Dimensional analysis

Flow characteristics on the rough bed are a function of fluid characteristics, physical characteristics of the bed, and hydraulic flow conditions. According to Figure 2-2, the effective

geometrical, kinematic, and dynamic variables during the jump on the undulating bed are as follows.

Geometric properties: roughness height (D), bed roughness distance (p), initial flow depth (H) and flow depth (y).

Kinematic Properties: Average Flow velocity (u_m) and Shear velocity (u*)

Dynamic Properties: Weight force (F_g) with gravity acceleration index (g) viscosity force (F_V) with dynamic viscosity index (μ), and motor force (F_I) with specific mass index (ρ).

The parameters affecting the hydraulic properties on the rough bed can be shown as follows.

$$f_l(H, y, u_m, u_*, p, D, g, \mu, \rho)=0 \quad (3\text{-}2)$$

In the function presented in Equation (2-2) there are nine independent variables with three main quantities of length, mass and time. Using dimensional analysis by Buckingham method, the following dimensionless function is obtained for the purpose of evaluating the flow on the rough bed.

$$f_2\left(Re, Fr_1 = \frac{u_m}{\sqrt{gH}}, \frac{H}{D}, \frac{P}{D}, y^+ = \frac{yu_*}{\nu}, u^+ = \frac{u_m}{u_*}\right) \quad (3\text{-}3)$$

In the above relation, Fr_1 is the initial Froude number and Re are the Reynolds number. By neglecting the effect of the conjugate due to the high Reynolds number and establishing the subcritical flow (0.25 - 0.25 0.10) in the tests, the relation (3-3) is simplified.

$$f_3\left(\frac{H}{D}, \frac{P}{D}, y^+ = \frac{yu_*}{\nu}, \frac{u_m}{u_*}\right) \quad (3\text{-}4)$$

In the above relation, $u^+ = \frac{u_m}{u_*}$ is shear dimensional velocity, $y^+ = \frac{yu_*}{\upsilon}$ the normalized effective height, P/D distance of roughness ratio and H/D submergence ratio. Assuming a submergence ratio in the specified range, the above relationship can be simplified to the following form.

$$f_4\left(\frac{P}{D}, y^+, \frac{u_m}{u_*}\right) \quad (3\text{-}5)$$

3-3- Numerical simulation of flow on rough bed

3.3-1- Network Range Flow

In order to simulate the flow, the desired range must first be networked. The network was created by Gambit software in three stages, respectively, geometric scope, networking and boundary condition definition.

The geometric range of the flow was defined as two-dimensional for the cylindrical substrate. The geometric range consists of the sides and edges and the coordinate points or nodes. The

geometrical boundary was created by defining the coordinates of the initial vertices and the edges and sides using these points (Soltani and Rahimi Asl, 2007).

In this research, the area of networking is 2 m long, 0.2 m high and 0.25 m wide. After defining the geometric range, the flow of this range was mapped. The networking features include the shape and type of elements. Given the conditions such as the corners, the type of elements suitable for the computational range is determined. Irregular square networks were used to network this area. This type of networking is used for boundaries in the form of a closed loop of sides. To create a network in the range, all sides of it must be networked at specified intervals. Figure 4-4 shows the computational domain networking.

The final step in networking involves determining the boundary conditions of the computational domain. For two-dimensional models, boundary conditions are defined for later dimensions of the network. Model type specifications were determined at the boundaries and within the range. Range specifications include two types of boundary and continuous area. According to Figure (3-4-a) the boundary conditions are defined as the inlet hydrostatic pressure, the outlet air pressure and the wall for the channel bed with a specified roughness.

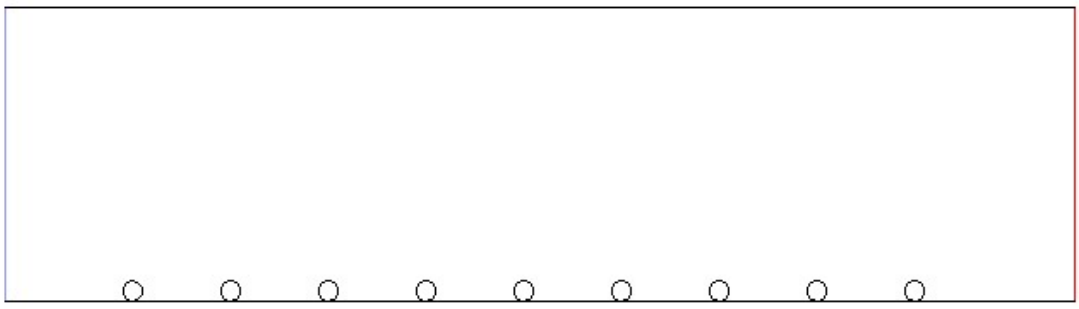

(a)

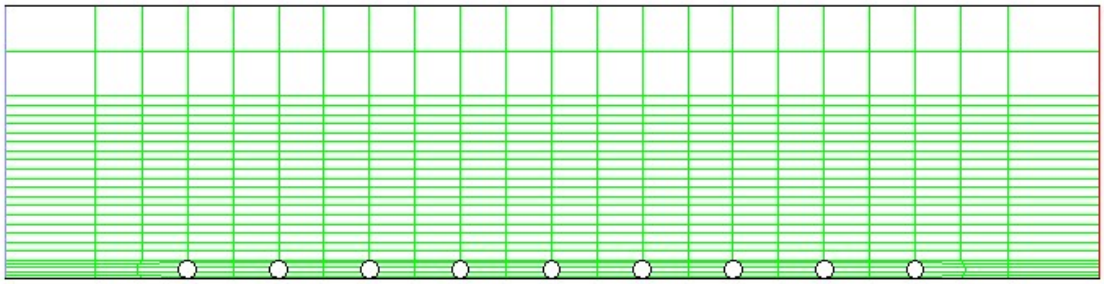

(b)

Figure 3-4- Schematic drawing of computational domain networking a) Geometric domain b) Area networking

The space within the computational domain is a continuous area that determines the physical properties of the model. The continuous area can be defined as fluid, porous and solid forms. Once the physical properties are known, the model of the equations used to determine it is determined. The continuous area is defined as fluid.

3.2.3 Finite volume method

The finite volume method was used as the finite difference formulation for development and main CFD applications through Fluent software. Fluent software for modeling fluid flow and heat transfer in complex geometric ranges. This software uses the finite volume method to transform the governing equations into algebraic equations (Soltani and Rahimi Asl, 2007). The numerical solution of these equations using the finite volume method involves the following steps:

- Overall integration of the equations governing the fluid flow over the control volumes related to the flow field.
- Discretization involves the placement of some kind of finite difference approximation for expressions within the integral equation that includes flow processes such as displacement, infiltration, and springs. Thus integral equations become a system of algebraic equations.
- Solving Algebraic Equations Using the Nonlinear Equation System Repeat Resolution Method.

Fluent software enables complete network switching and flow analysis for complex geometries. Changing the network and analyzing the flow with the irregular network is possible with this software. Network control is one of Fluent's advanced capabilities, which gives the user complete information about the number of cells and the designation of non-networked spaces within the computational range. Network information includes the range, maximum and minimum of the network in the coordinates and volume of cells.

It is also possible to improve the network, including fine-tuning the network at the required boundaries and locations. Optimization of the network results in more accurate gradient regions such as boundary layer (Khademi et al., 2005).

3.3.3- Selecting a computational method

The numerical model consists of two separate and continuous solver methods for solving integral equations of mass and momentum survival. In the present study, a separation method is used in which the governing equations of continuity, momentum, and turbulence are solved in order, and since these nonlinear equations have to be repeated several times in the solution process loop before obtaining the convergent solution.

In the separation method of continuum and momentum equations in integral form is as follows:

$$\oint \rho v dA = 0 \quad (3\text{-}6)$$

$$\oint \rho v v.dA = -\oint pI.dA + \oint \tau.dA + \int_V F dV \quad (3\text{-}7)$$

Where I is the homogeneity matrix, τ stress and F is the force vector (Soltani et al., 2007). Also, time analysis of continuous equations was performed by implicit time method.

The discretization of the momentum equation is given by the third-order Quick and MUSCL methods. These methods are compatible for mixed or irregular networks. The third-order methods are based on the computation of the mean in the second-order method and the central mediation for the variables. For e, according to Figure 3-5, the values of the unknown variables are determined from the following relation.

$$\phi_e = \theta\left[\frac{S_d}{S_c + S_d}\phi_P + \frac{S_c}{S_c + S_d}\phi_E\right] + (1-\theta)\left[\frac{S_u + 2S_c}{S_u + S_c}\phi_P + \frac{S_c}{S_u + S_c}\phi_W\right] \quad (3\text{-}8)$$

In third-order methods the value of the variable θ is equal to 1/8.

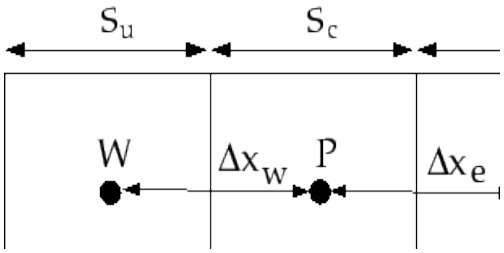

Figure 3-5 - One-dimensional control volume

In the MUSCL method, the unknown variable values can be obtained from:

$$\phi_f = \theta\phi_{f,CD} + (1-\theta)\phi_{f,SOU} \quad (3\text{-}9)$$

In this respect, the second-order upwind method is determined as follows:

$$\phi_{f.CD} = \frac{1}{2}(\phi_0 + \phi_1) + \frac{1}{2}(\nabla\phi_o \cdot \vec{r}_0 + \nabla\phi_1 \cdot \vec{r}_1) \quad (3\text{-}10)$$

$$\phi_{f.SOU} = \phi + \nabla\phi \cdot \vec{r} \quad (3\text{-}11)$$

Where subscripts 0 and 1 belong to cells that have a common f-face. $\nabla\phi_o$ and $\nabla\phi_1$ are the gradients produced in cells 0 and 1, and $\vec{r}$ is the vector along the center of the cell to the center of the face (Unnamed, 2006).

Since the equations to be solved are nonlinear, control of ϕ_0 changes seems necessary. The Under-relaxation coefficients α are used to correct the values of the variables calculated in each iteration. In simulation of flow on rough bed for stable or convergent behavior the following factors are modified and the default values for pressure, momentum, k and ε are changed to about 0.5, 0.3, 0.5 and 0.5.

Discretization of the pressure values by the Body Force Weighted method. The pressure in the equations is calculated by assuming that the vertical gradient is the constant between the pressure and the volume forces. Since the forces of pressure in the initial conditions of the solution are known to be appropriate (Unnamed, 2006).

The velocity-pressure coupling in the separation method is created using the PISO (Pressure-Implicit with Splitting of Operators) algorithm. In this method, after solving the pressure equation, the velocity values and their corresponding discharges are inserted into the momentum equation and repeated until the momentum equilibrium is calculated.

3-3-4-Basic turbulence equations and flow phases

In this study, the RNG k-ε model is used. RNG k-ε models based on flow characteristics on the rough bed are a function of fluid properties, bed physical properties, and hydraulic flow conditions, modeling kinetic energy and energy dissipation of eddy turbulence. This model shows good agreement with the laboratory results.

In turbulent currents the velocity fields are greatly influenced by the walls. Modeling near the bed has a great impact on the accuracy of numerical methods. Because the walls are the source of eddy and turbulence. There is also a large gradient near the wall of the flow variables and momentum transfer occurs there. Standard wall function model was used to study the flow behavior.

The flow on the rough bed is biphasic. Free-flow simulation was performed with VOF fluid volume component model. In the fluid volume component model, the seasons between two climate phases were determined by geometric reconstruction. In the discrete models, the Courant number for the fluid volume component model is set to 0.25 (Khademi et al., 2005).

3.3-5 Define the boundary and initial flow conditions

The boundary conditions are specified in the Gambit software. If the values of variables are introduced in Fluent software. Inlet boundary conditions are introduced as hydrostatic pressure in which the pressure p at different depths h is equal to the distance from the water surface (the origin of the coordinates) upstream of the flow. Also in this boundary the parameters of turbulence intensity I and hydraulic diameter of R_h were calculated. The turbulence intensity at the inlet boundary depends on the flow conditions. The turbulence intensity is low and the turbulence intensity can be high or low if the current is not developing. The intensity of the turbulence in the channels in the developed condition is determined by the following relation (Anonymous, 2006).

$$I = \frac{\sqrt{u'u' + v'v'}}{u_1} = \frac{u'}{u_{ave}} = 0.16(\mathrm{Re}_{DH})^{-1/8} \quad (3\text{-}12)$$

In this respect the Reynolds number flows at the inlet boundary. Turbulence intensity values were in the range of 3.5 to 4.5% and hydraulic diameter was 0.04 to 0.05 m.

The boundary condition of the walls is used to constrain the computational areas. In the canal bed, the boundary condition of the wall was assumed to be zero. Inlet boundaries were determined in terms of the phases of climate flow. The computational space interior is defined as a mix of climate

6.3.6.6 Define physical properties of materials and operating pressure

Material properties were defined as density, viscosity, heat capacity, thermal conductivity, mass diffusion coefficient and kinetic theory parameters. The type of material was introduced into the model as a fluid fluid and the properties of the material were introduced by copying from the database.

Relative pressure is always used in calculations. Incompressible and free-flow calculations, the average pressure value is used. The default operating pressure is 101325 Pascal. The acceleration of gravity along the vertical axis of y was defined as -9.8 m/s^2.

3.3-7- Initial guess of the flow field

Prior to the numerical simulation, the initial values of the current including the boundary of computation start, average values of pressure, flow rate, kinetic energy and energy dissipation were introduced. In order to solve the problem with high accuracy and convergence, the initial water fluid conditions for the upstream cells from the beginning of the computational space to the first roughness and from the bottom to the water surface depth were selected and the fluid volume component was defined as one.

3.3-8- Performing flow calculations

The type of flow in the simulation of the flow on the rough bed is unstable. Time step size is 0.0001 seconds

Was considered. During the dissolution process, the convergence can be actively observed by checking the residuals, values of forces and surface integrals. The convergence of the calculations under the influence of the factors can be stopped. The large number of cells and factors below the attenuation are the most complex causes of non-integrationism. Some numerical control methods and modeling techniques such as disaggregation or pressure-velocity communication methods and sub-discounting parameters are used to increase convergence.

At the end of each iteration, the sum of the residuals was calculated and stored for each flow variable. The residuals were considered as 0.001 for each of the variables of depth, flow rate and kinetic energy and energy dissipation. The solution stops automatically when each variable reaches the specified convergence criterion. Time elapsed can also be seen in unstable currents.

3.3-9- Model Operating Process

The process of solving the model is simple. The process is summarized as follows:

- Create model grids
- Network file transfer
- Network checking and optimization
- Selection of physical models
- Definition of material properties
- Determine performance conditions
- Determine boundary conditions
- Determine initial conditions
- Adjust analysis controls
- Convergence setting
- Perform calculations and show convergence

• Post-processing including drawing profiles and meters and engineering analysis

The general operation steps in the model are as shown in Algorithm Figure 3-6 (Unnamed, 2006).

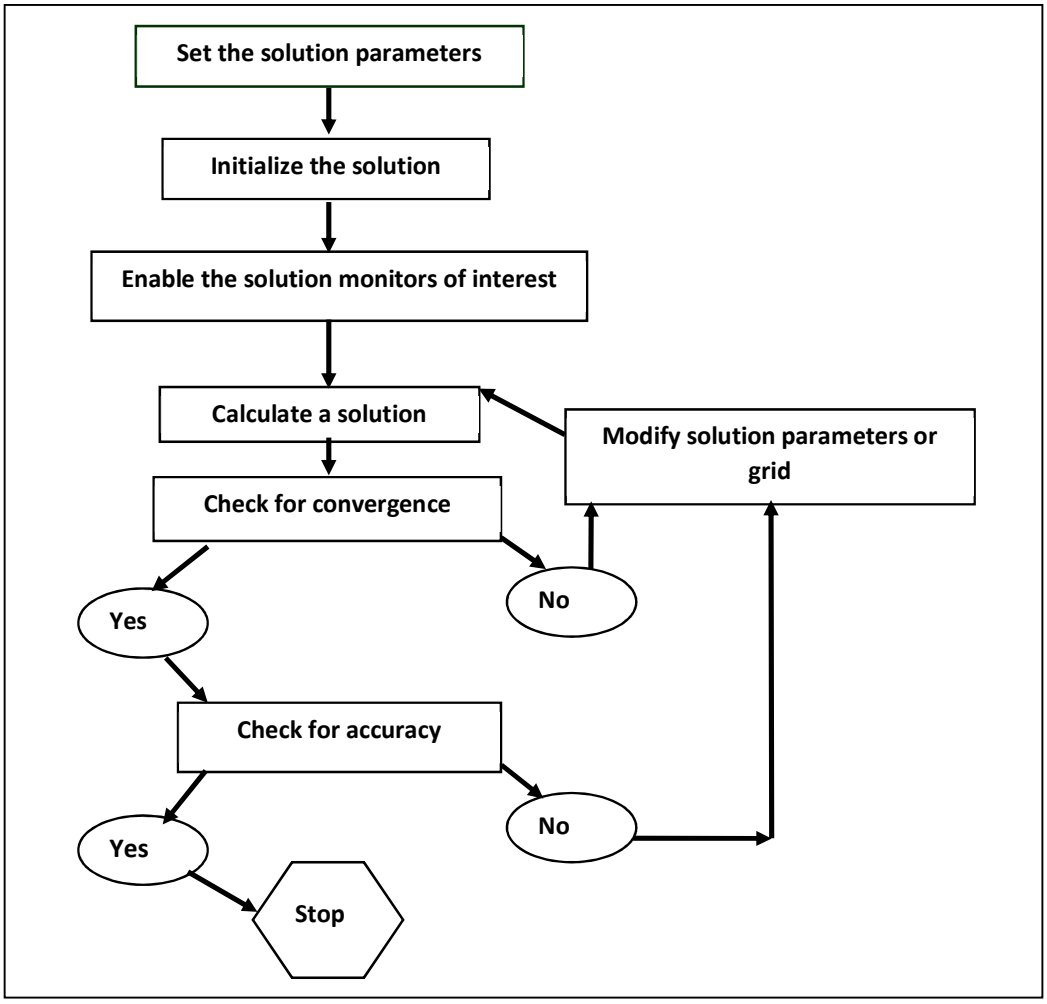

Figure 3-6- Model Operational Stage Algorithm

3.3-10- Create input and output file

Gambit software is used to generate all kinds of regular and irregular networks and to create networking files. The networking files are stored in the Gambit application in mesh format. Fluent can read mesh files. The simulation information is stored in two files with Case and Data extensions in both text and binary formats.

Case files include grid, boundary conditions, and parameters for the problem. Data files contain the values of the flow field in each grid cell and the numerical residuals for that flow field. Case and Data files can be automatically saved at a specified interval during resolution. This will be useful in problems that are solved in an unstable manner.

3.3-11- Adaptation and optimization

An important advantage of irregular networks is the ability to perform adaptation and network optimization. This feature can be added to any part of the network that needs more cells. Adding these cells improves the flow field resolution and converges faster. In the present study, two types of Region and wall Adaption y^+ were used. In the region matching, the minimum volume of cells near the walls was reduced by 1×10^{-5}. Adaptation y^+ is a criterion for shrinking and enlarging the grid near the wall during program execution. A parameter is dimensionless and is defined in the form of the following relation.

$$y^+ = \frac{\rho u_* y_P}{\mu} \quad (3\text{-}13)$$

In this respect, $u_* = \sqrt{\tau_0 / \rho_w}$ is shear velocity, τ_0 is shear stress of the wall, y_P p-distance from the wall, ρ and μ are the specific mass and viscosity at the p-point.

Turbulence models are recommended for standard wall functions and the unbalanced function $300>y^+>30$ (Unnamed, 2006).

3.3-12- Generate images and charts and report on the solution

In this software images are generated for viewing networks, contours, profiles and so on. The grid or outline of the problem for all or part of the domain can be viewed using the grid display panel. Drawing contours or profiles of velocity, kinetic energy, and energy dissipation in the physical domain is possible using the model (Khademi et al., 2005).

Speed vectors can be plotted for the entire computational range. The velocity vectors are plotted in the center of the cell with the length and color that represent the cell profile. The distance between vectors and their color and size can be changed.

For drawing the grid, model display colors were improved. This capability helps to better understand the model. Drawing contours and profiles are continuous and complete. The number of contours or profiles on the surface area should be stated. In biphasic currents the minimum value of 2 levels is considered. XY graphs are plotted using data in one or more regions and the model results can be compared with the experimental results. In order to draw profiles and graphs with dimensionless coordinates, the data needed to be transferred to Excel graphics software and the necessary parameters created.

For the selected boundary zones, the mass flow rates, tensile forces, momentum and mean mass flow rates can be obtained at one level. Reports containing models and boundary conditions and the solution method can be stored in a file.

3.4- Turbulent flow structure

Since Reynolds stress model is suitable for spin, eddy and secondary flows in channels (Luis, 2008), this study was used to simulate the flow on rough bed. In this model, five equations including transition equations for Reynolds stresses and energy dissipation equation are solved.

The Reynolds stress model is used to investigate turbulence intensities, kinetic energy and energy dissipation. The intensity of turbulent stresses at different depths and cross sections on the bed is roughly $\sqrt{\overline{v'^2}}$ and $\sqrt{\overline{u'^2}}$ (Lewis, 2008). The intensity of Reynolds stress $(\overline{u'v'})_m$ at different Froude numbers is investigated.

3.4-1- Kinetic energy of turbulence

The kinetic energy of the turbulence using the Reynolds stress tensor is obtained from the following relation:

$$k = \frac{1}{2}\overline{u_i' u_j'} \quad (3\text{-}14)$$

The turbulence kinetic energy transfer equation is used as follows.

$$\frac{\partial}{\partial t}(\rho k) + \frac{\partial}{\partial x_i}(\rho k u_i) = \frac{\partial}{\partial x_j}\left(\left(\mu + \frac{\mu_t}{\sigma_k}\right)\frac{\partial k}{\partial x_j}\right) + \frac{1}{2}(P_{ii} + G_{ii}) - \rho\varepsilon\,(1 + 2M_t^2) + S_k \quad (3\text{-}15)$$

In the above relation $\sigma_k = 0.82$.

3-4-2- Energy depreciation rate

The energy dissipation tensor is obtained from the following equation.

$$\varepsilon_{ij} = \frac{2}{2}\delta_{ij}(\rho\varepsilon + Y_M) \quad (3\text{-}16)$$

In the above term, $Y_M = 2\rho\varepsilon M_t^2$ is the thermal expansion of the damping. M_t The turbulence Mach number is determined from the following equation.

$$M_t = \sqrt{\frac{k}{a^2}} \quad (3\text{-}17)$$

Where a is the speed of sound.

The scalar value of the energy dissipation rate is calculated using a transfer equation similar to the standard k-ε model.

$$\frac{\partial}{\partial t}(\rho\varepsilon) + \frac{\partial}{\partial x_i}(\rho\varepsilon u_i) = \frac{\partial}{\partial x_j}\left[(\mu + \frac{\mu_t}{\sigma_\varepsilon})\frac{\partial\varepsilon}{\partial x_j}\right] + C_{\varepsilon 1}\frac{1}{2}(P_{ii} + C_{\varepsilon 3}G_{ii})\frac{\varepsilon}{k} - C_{\varepsilon 2}\rho\frac{\varepsilon^2}{k} + S_\varepsilon \quad (3\text{-}18)$$

Experimental coefficients of the standard k-ε model include $C_{\varepsilon 1}$ = 1.44, $C_{\varepsilon 2}$ = 1.92, $C_{3\varepsilon}$ = -1, and σ_k =1.

Also in the Reynolds stress model the eddy viscosity turbulence model $\mu_t = \rho C_\mu \frac{k^2}{\varepsilon}$ is determined in terms of kinetic energy values, the rate of energy dissipation and the viscosity coefficient C_μ is 0.09 (Unnamed, 2006).

3-4-3- Turbulent Diffusive Transport

The Turbulent Diffusive Transport $D_{T,ij}$ can be modeled as follows.

$$D_{T,ij} = C_s \frac{\partial}{\partial x_k}\left(\rho \frac{k}{\varepsilon}\overline{u'_k u'_l}\frac{\partial \overline{u'_i u'_j}}{\partial x_l}\right) \quad (19\text{-}19)$$

The simplest form of the above equation for determining scalar turbulence propagation is as follows:

$$D_{T,ij} = \frac{\partial}{\partial x_k}\left(\frac{\mu_t}{\sigma_k}\frac{\partial \overline{u'_i u'_j}}{\partial x_k}\right) \quad (3\text{-}20)$$

3-5 Indicators for evaluation of numerical simulation model

Different statistical criteria are used to check the accuracy of the numerical simulation model between the observed data and the computational results. One of these criteria is the mean relative error of RAE, which was determined based on the following equation.

$$RAE = \frac{\sum_{i=1}^{n} |(y_{oi} - y_{ci})|}{\sum_{i=1}^{n} y_{oi}} \quad (3\text{-}20)$$

In the above relations, the y_{ci} parameter is simulated, the y_{oi} is the calculated parameter in time step i with n parameters.

Fourth Chapter

Results and Discussion

4-1- Introduction

In this study, both experimental and numerical methods were used to investigate the velocity profiles on the rough bed. In the experimental method, the effect of hydraulic flow conditions was investigated on the geometrical dimensions of the bed including height and distance of the bed roughness and the depth of flow on the flow characteristics. Experiments were necessary for empirical investigation. These tests were performed in a laboratory flume.

Numerical simulations of the flow on the coarse bed in this study were performed using k ε RNG turbulence models. The free water level was determined by numerical method of VOF fluid volume fraction. The velocity profiles, bed shear velocities and bed shear stresses in different turbulence models have been determined and compared with the experimental results.

In this chapter, the results of the laboratory investigation and numerical modeling of the flow on the rough bed are presented and discussed. For ease of conclusion and discussion, the results of the study are presented in two separate sections, including laboratory investigation and numerical modeling.

4-2- Laboratory test results

As discussed in Chapter 3, the effects of physical and hydraulic parameters on velocity profiles as in Equation (3–5) include dimensionless shear velocity and dimensionless depth in cylindrical rough substrates.

4.2.2 Experimental data

As described in section (3-1-1), 12 series of measurements were performed on 6 types of rough bedding with different dimensions and different roughness intervals according to Table (3-1).

4.2.2 Water level profiles

The results of the direct measurement of the flow depths at different points in the flow in the central axis of the flume have water surface profiles. Water surface profiles were used to determine the slope of Sw surface water, bed shear stress values τ_0 and drag coefficient of flow. Figures (1-4) to (4-4) show the free water surface profiles of the various tests. In these figures, the S_W water slope was calculated by fitting the line to the observed water level data and the relationship of bed shear stress was calculated using $\tau_0 = \gamma R S_w$.

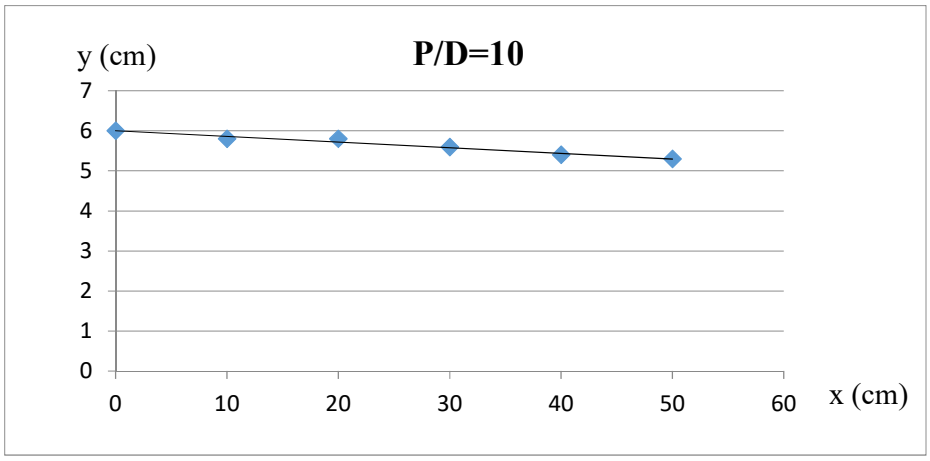

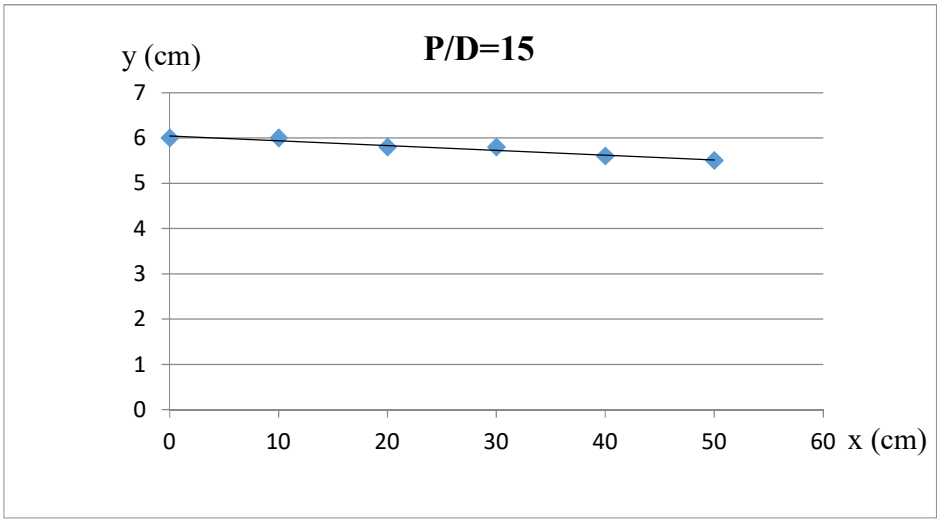

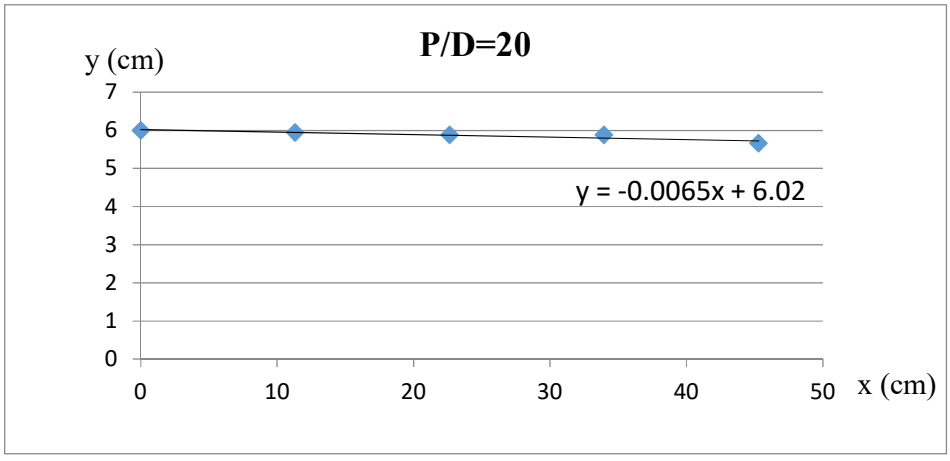

Figure 4.1- Surface profiles of cylindrical substrates (H = 6 cm, D = 6 mm)

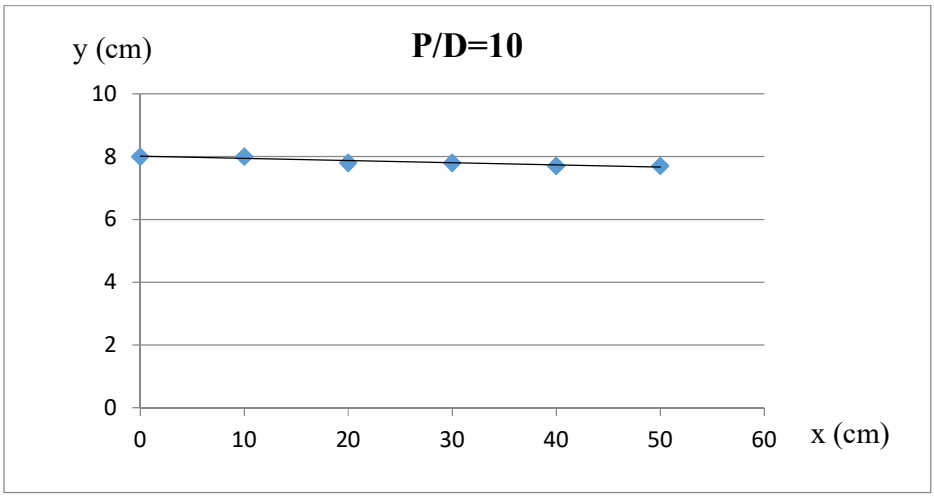

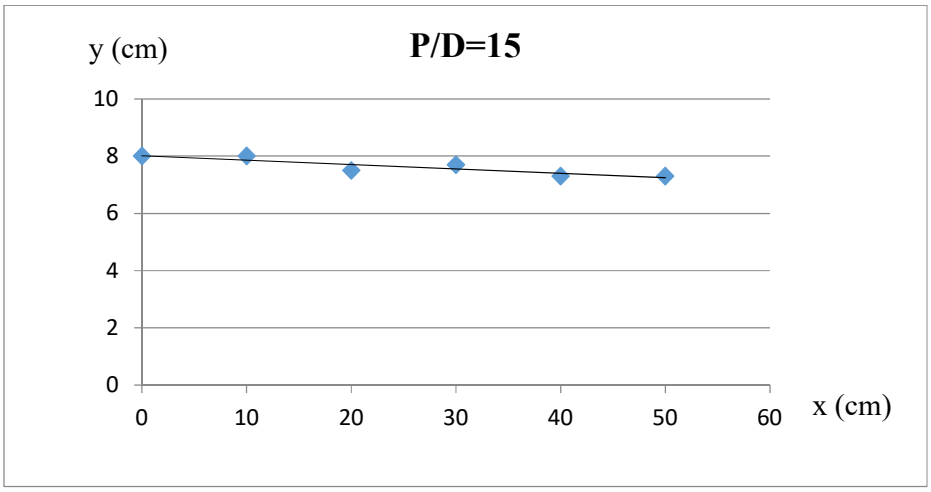

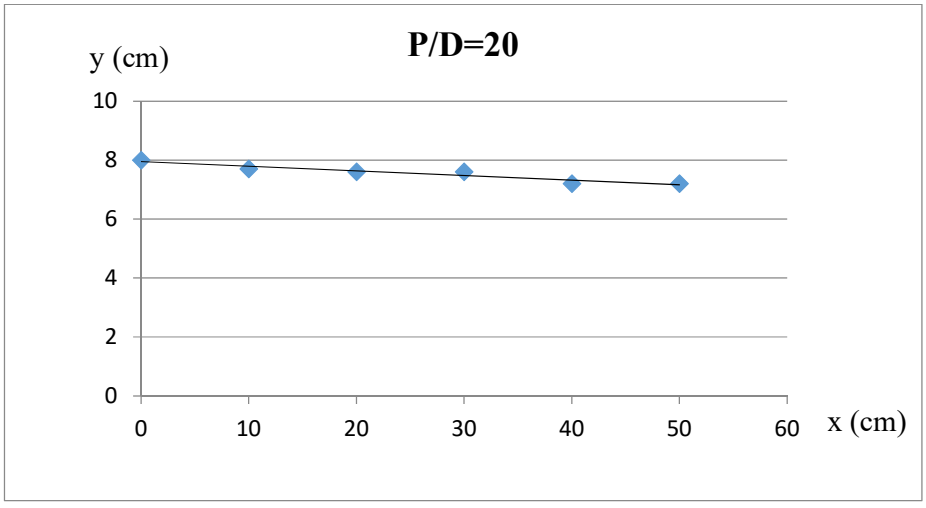

Figure 4-2- Surface profiles of cylindrical substrates (H = 8 cm, D = 6 mm)

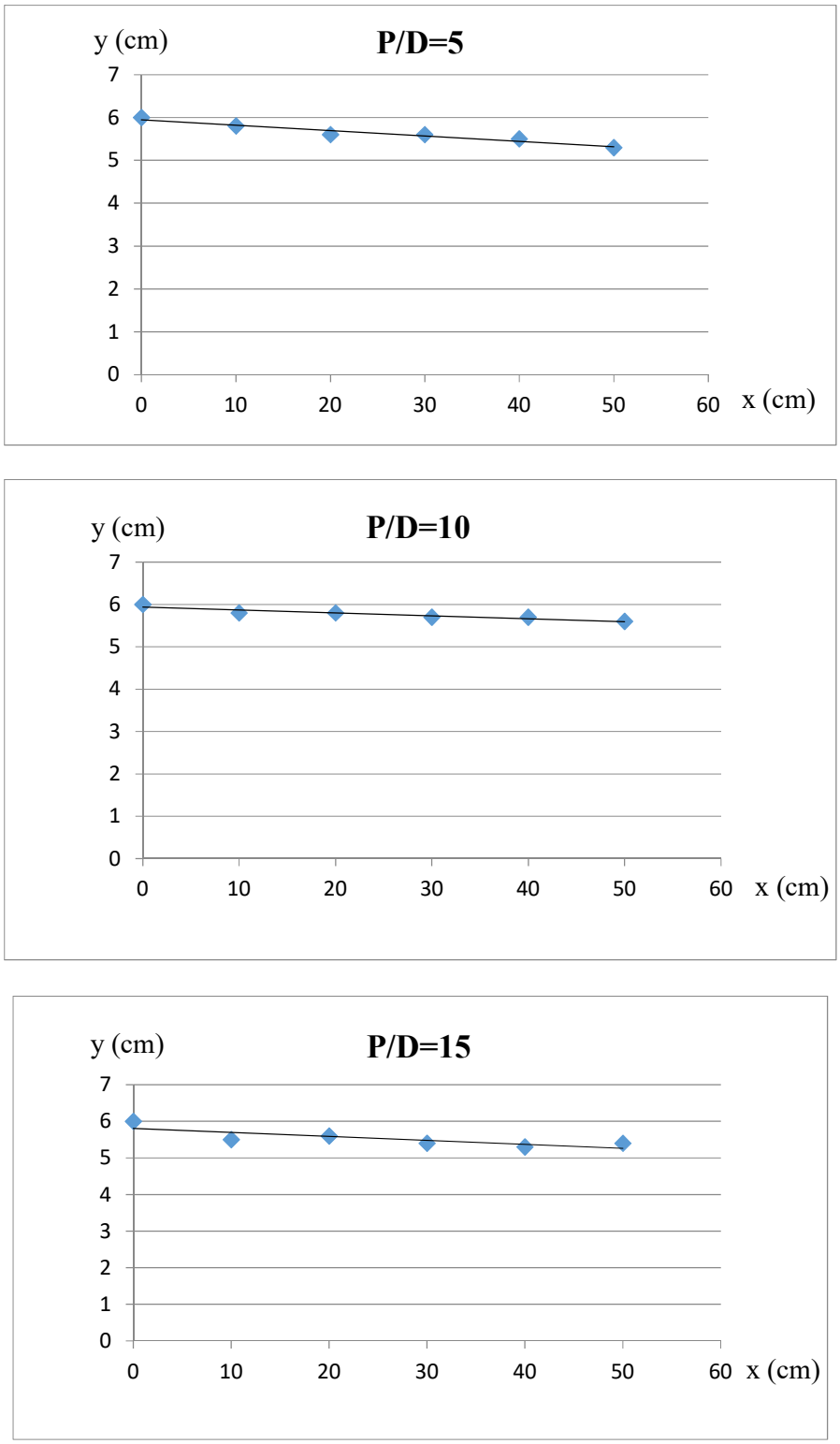

Figure 4-3- Surface profiles of cylindrical substrate (H = 6 cm, D = 10 mm)

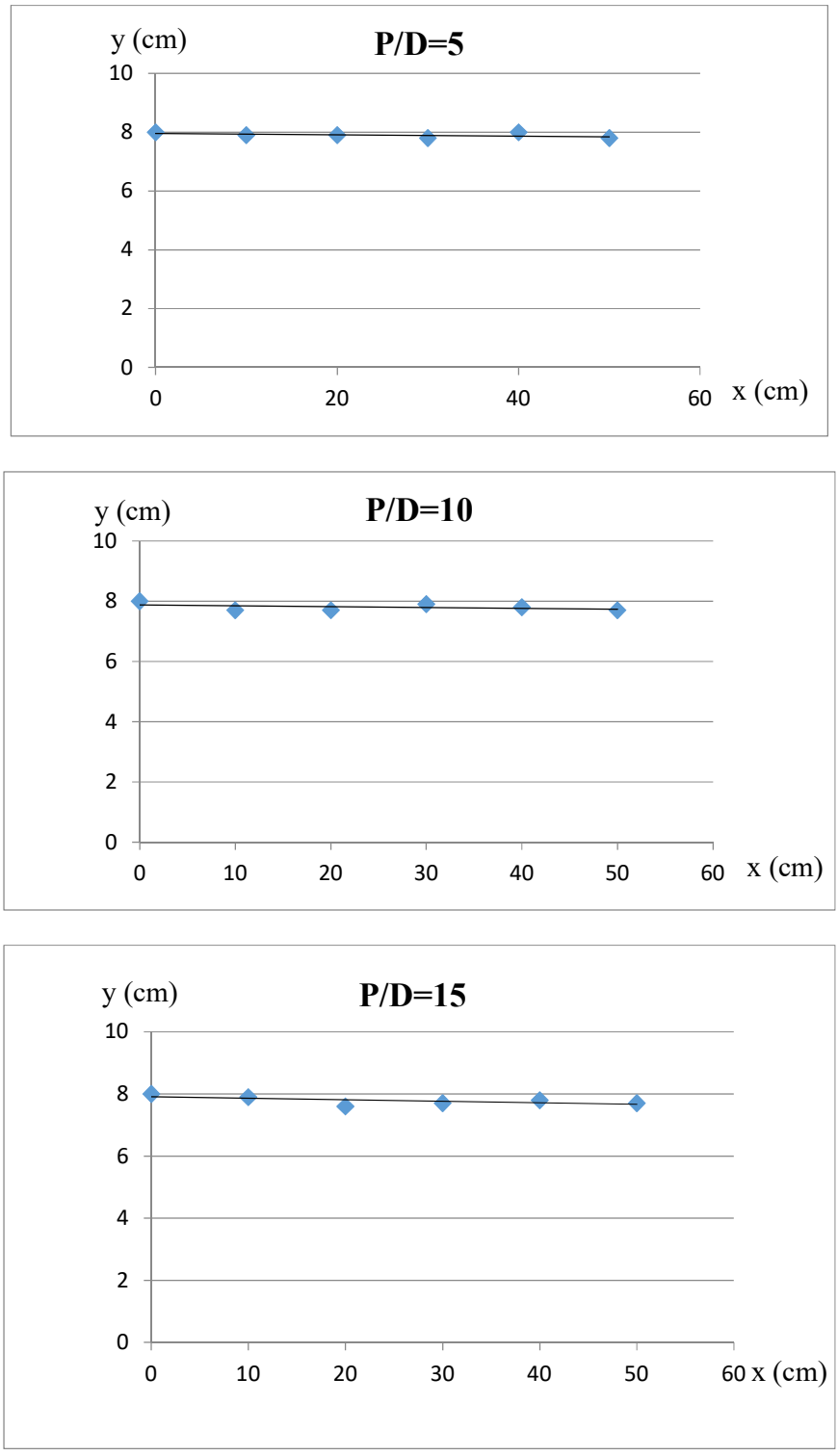

Figure 4-4- Surface profiles of cylindrical bed (H = 8 cm, D = 10 mm)

4.2.2 Velocity profiles

In this study, velocity profiles were measured in different tests on rough substrates. In Figures (4-5) to (4-7) measured profiles for rough cylindrical substrates with heights of 6 and 10 mm

and water depths of 6 and 8 cm at Different distances are displayed. In these profiles the velocity changes are logarithmic and the velocities increase with increasing distance from the beginning of the substrate (x) due to the decrease in depth (increase in energy loss) downstream. In the rough substrates, the dimensional values of the velocity show less variation during the flow (x).

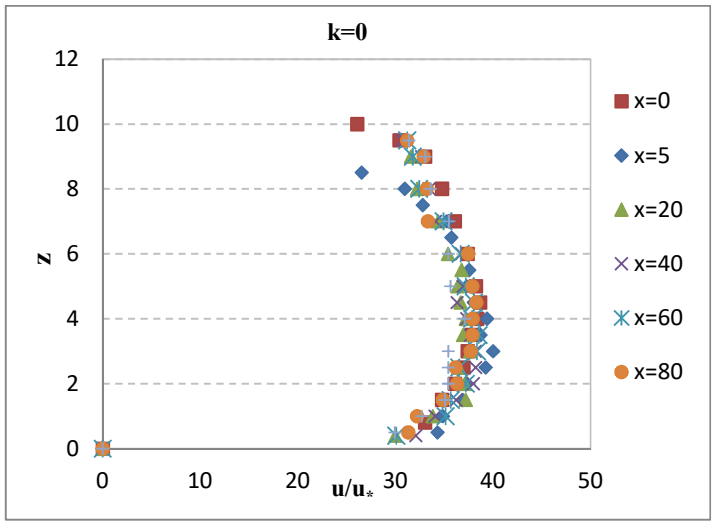

Figure 4-5- Speed profiles along the bed without roughness (Abbaspour, 2014)

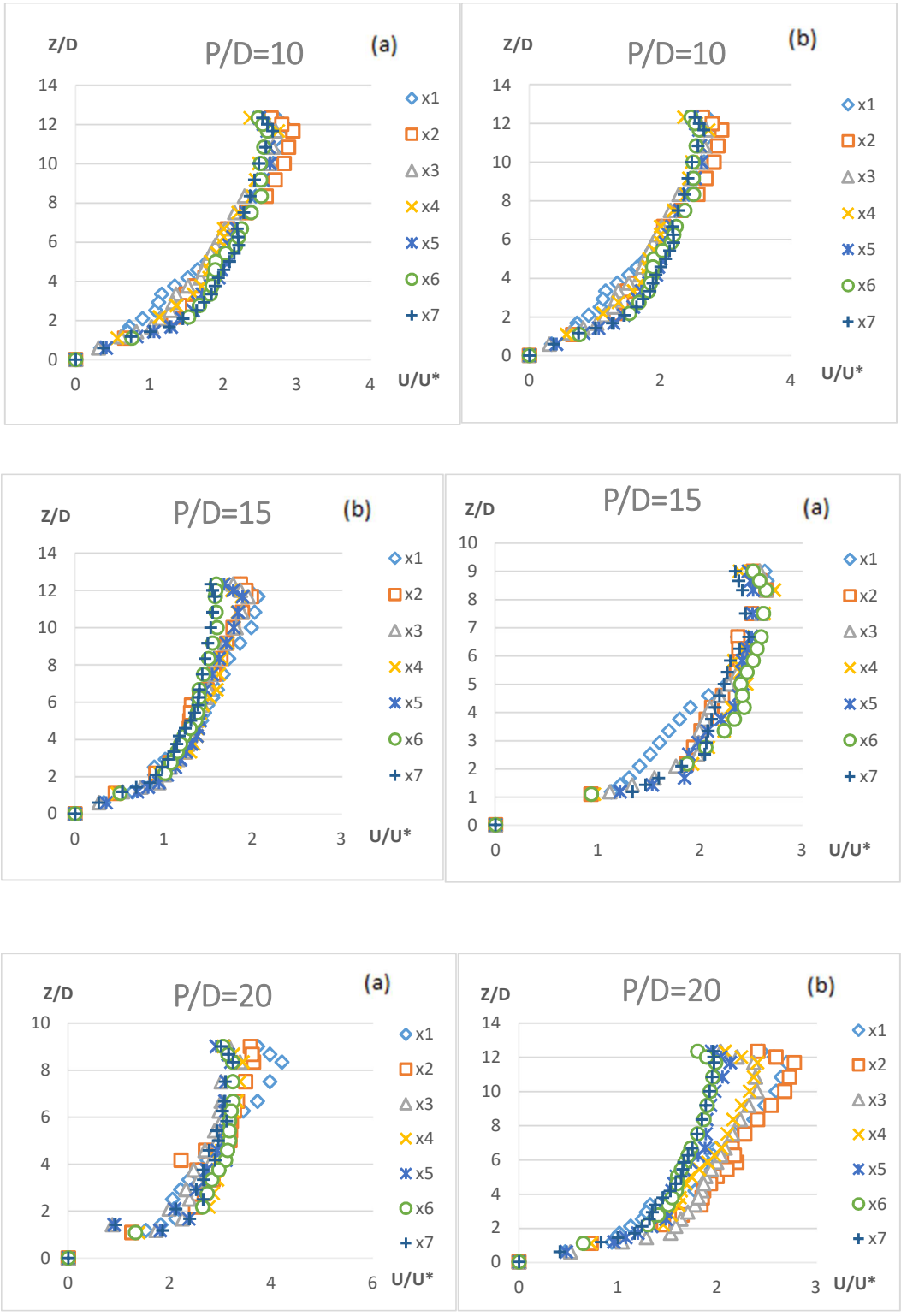

Figure 4-6- Dimensional velocity profiles along the cylindrical bed of a) H = 6 cm and b) H = 8 cm (D = 6 mm)

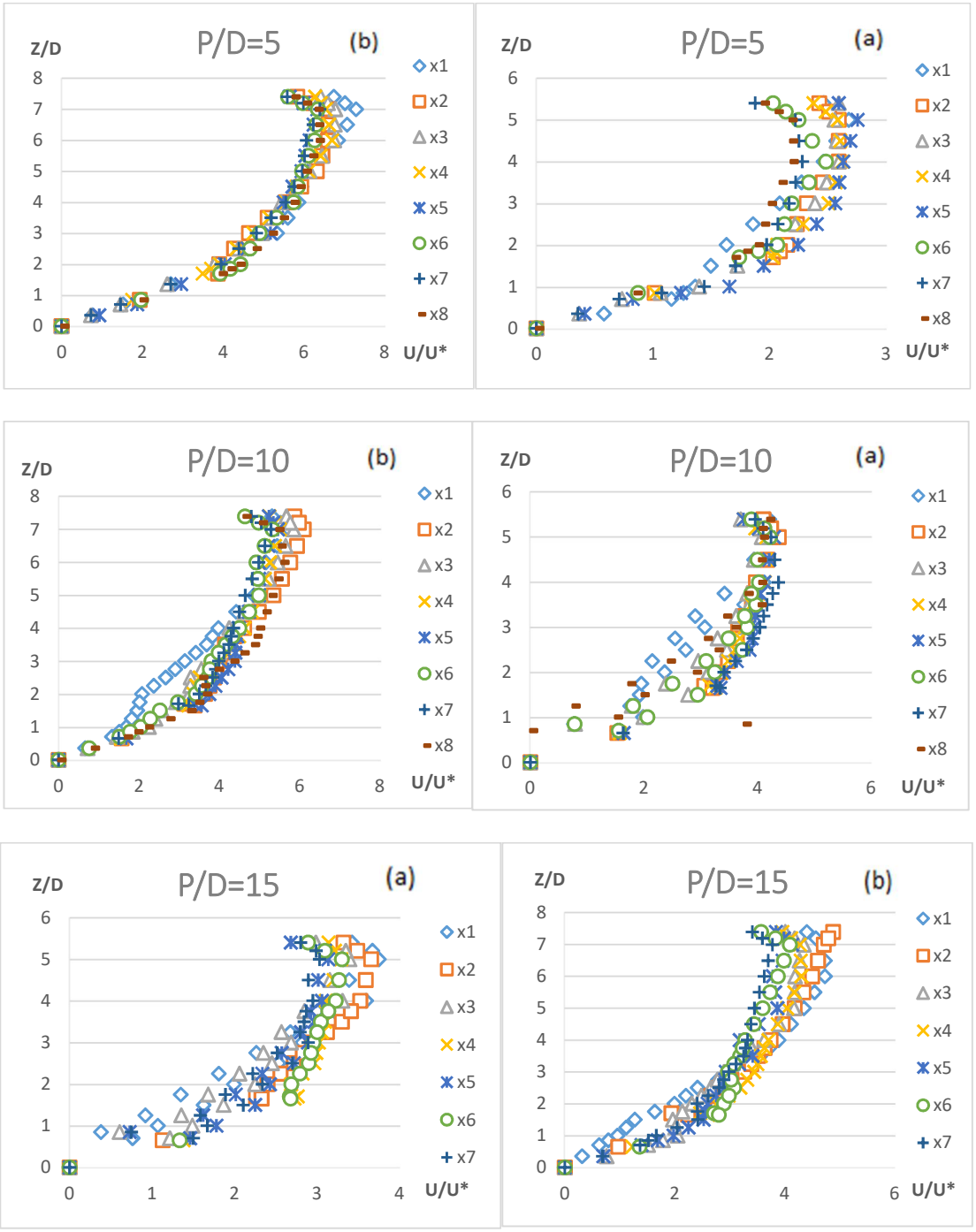

Figure 4-7- Dimensional velocity profiles along the cylindrical bed a) H = 6 cm and b) H = 8 cm for (D = 10 mm)

In Figures (4-8) and (4-9) the dimensional profiles of velocity $U^{+}= U/U_{*}$ for the dimensionless depth $y^{+}=yu_{*}/\nu$ for cylindrical roughnesses of height Shown are 6 and 10 mm. As can be seen in these figures, the velocity profile is logarithmic and follows the following general relation:

$$\frac{u}{u_*} = \frac{1}{k} Ln \frac{u_* y}{\vartheta} + A - \Delta U^+$$

(4-1)

Also in any of the forms (4-8), (4-9), (4-10) and (4-4) can be deduced that by increasing the roughness intervals (P) the values of the dimensional velocities Is increasing. By comparing Figures (4-8) and (4-10) since the depth of water for the roughnesses of 6 and 10 mm is equal to 6 cm, the values of the dimensionless velocities in the bed with the roughness 10 mm longer than roughness 6 mm. Also by comparing Figures (4-9) and (11-4) it can be concluded that the values of dimensionless velocities in the bed with a thickness of 10 mm are greater than the thickness of 6 mm.

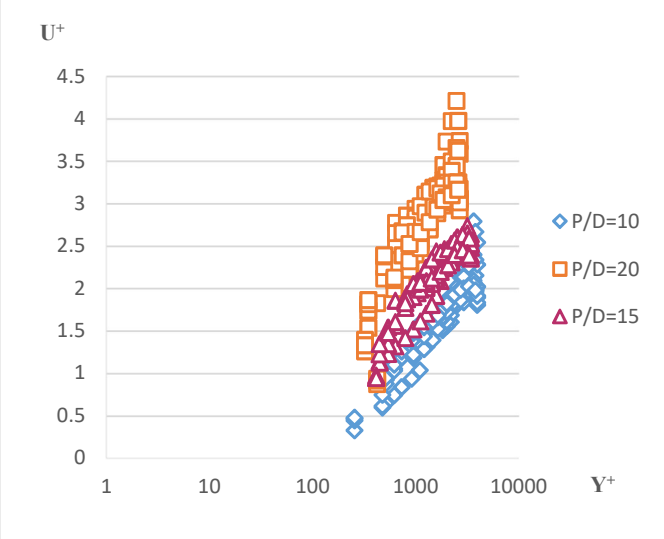

Figure 4-8- Dimensional velocities per y + in the bed with cylindrical roughness for D = 6 mm and H = 6 cm

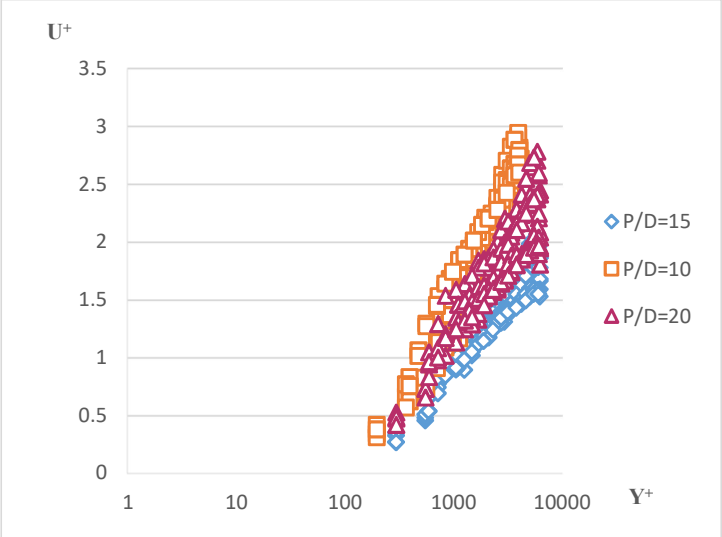

Figure 4-9- Dimensional velocities per y + in the bed with cylindrical roughness for D = 6 mm and H = 8 cm

In Figures (4-10) and (4-11), the dimensional profiles of velocity U^+ for dimensionless depth y^+ for cylindrical roughness of height 10 and water depths H =6 and H =8 As shown in these figures, the velocity profile is logarithmic, and the dimensionless velocity values for the water depth H=8 cm are greater than the depth of 6 cm.

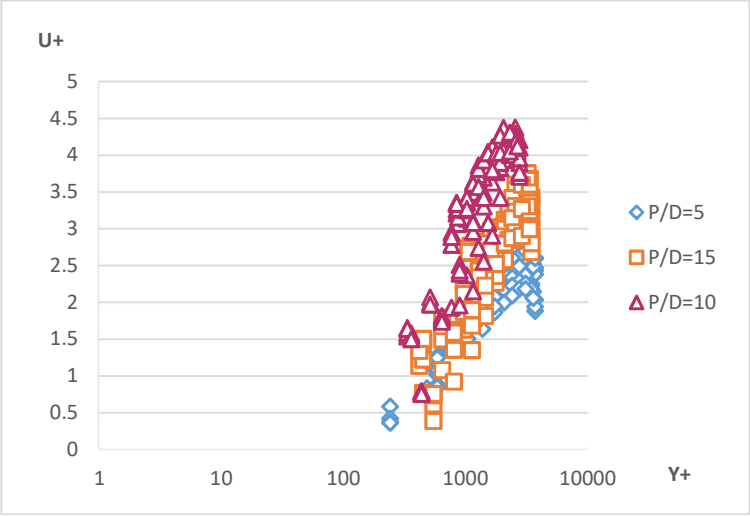

Figure 4-10- Dimensional velocities per y + in the bed with cylindrical roughness for D = 10 mm and H = 6 cm

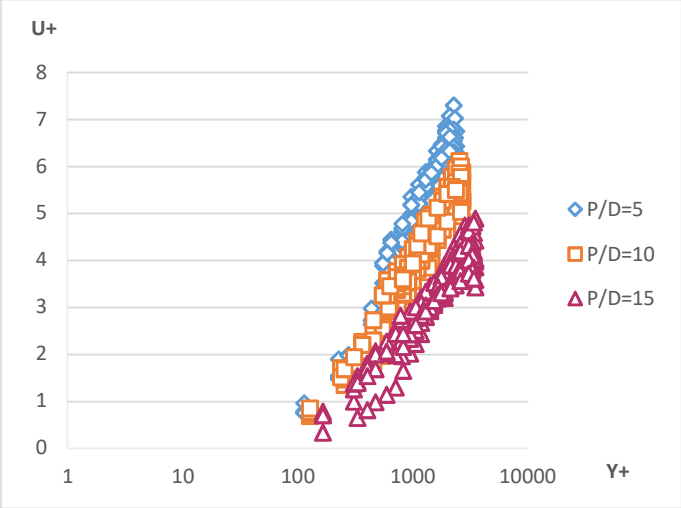

Figure 4-11- Dimensional velocities per y + in the bed with cylindrical roughness for D = 10 mm and H = 8 cm

4-2-4- Shear stress of the bed

The shear stress of the rough bed is determined using the momentum relation. The momentum equation at the beginning and end of the rough bed is as follows.

$$(M_2 + P_2 - S_2) = (M_1 + P_1 - S_1) - \int_{x_1}^{x_2} \tau_b dx \quad (4\text{-}2)$$

In this respect, P1, P2, M1, M2, S1 and S2 are the compressive forces, momentum, and normal stress forces, respectively, at the beginning and end of the interval. By omitting the normal stress forces in the relationship (2–3), the sum of the bed shear forces is obtained using the following relation (Kahn and Stefler 1996).

$$F_\tau = \int_{x_1}^{x_2} \tau_b dx = (P_1 - P_2) + (M_1 - M_2) \quad (4\text{-}3)$$

In the above relation, $P_1 = 0.5\gamma y_1^2$, $P_2 = 0.5\gamma y_2^2$, $M_1 = \rho u_1^2 y_1$ and $M_2 = \rho u_2^2 y_2$ is obtained for the values of depth and velocity at the beginning and end of the interval.

The shear stress of the entire bed in units of width is obtained from the following relation.

$$F_\tau = \int_{x=0}^{L} 0.5 c_f \rho u_m^2 \Delta x \quad (4\text{-}4)$$

Where C_f is the total surface drag coefficient and u_m the average velocity at each cross-section.

Figures 12-12 to 13.4 illustrate the variation of the drag coefficient for cylindrical roughness of 6 and 10 mm in height (H = 6 cm, H = 8 cm) at different distances. According to these

figures, as the roughness intervals (P) increase, the values of the drag coefficient and the coefficient of friction decrease. Also in all roughnesses the drag coefficient decreases downstream.

Table (1-4) shows the average values of the drag coefficient for each roughness. Maximum drag coefficient for cylindrical bed with 6 mm height, P / D = 15 and H = 8 cm depths was 0.515 and minimum drag coefficient for 10 mm height, intervals P / D = 15 and H = 8 cm depth is 0.05. Also, the average drag coefficient for the rough bedding is 0.002 which is much lower than rough bedding (Abbaspour & Farsadizadeh, 2012). In Table (4-1) the values of ΔU + for different roughness are shown. Generally, with increasing roughness intervals (P / D) the value of ΔU + decreases and the average ΔU + in roughness of 10 mm height is greater than the roughness of 6 mm height.

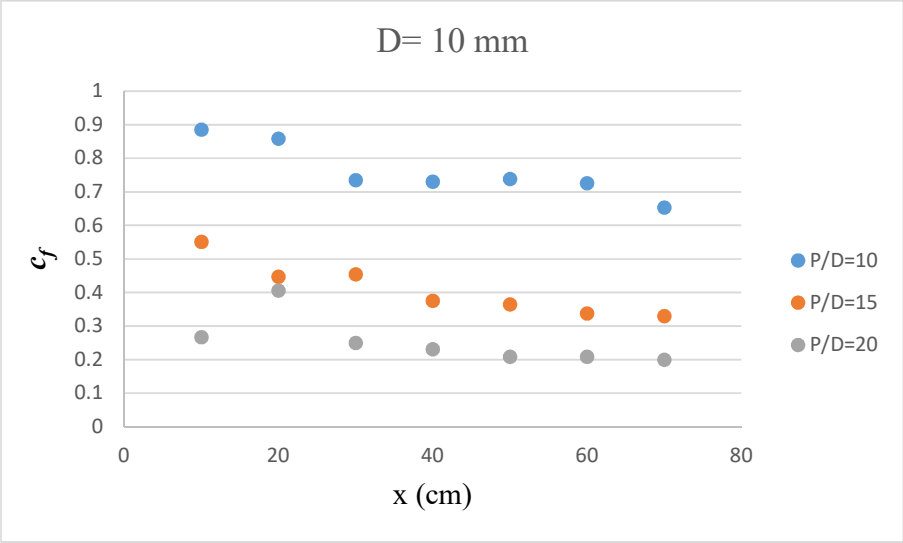

Figure 4-12- Drag coefficient Cf changes along the cylindrical bed for D = 10 mm and H = 6 cm

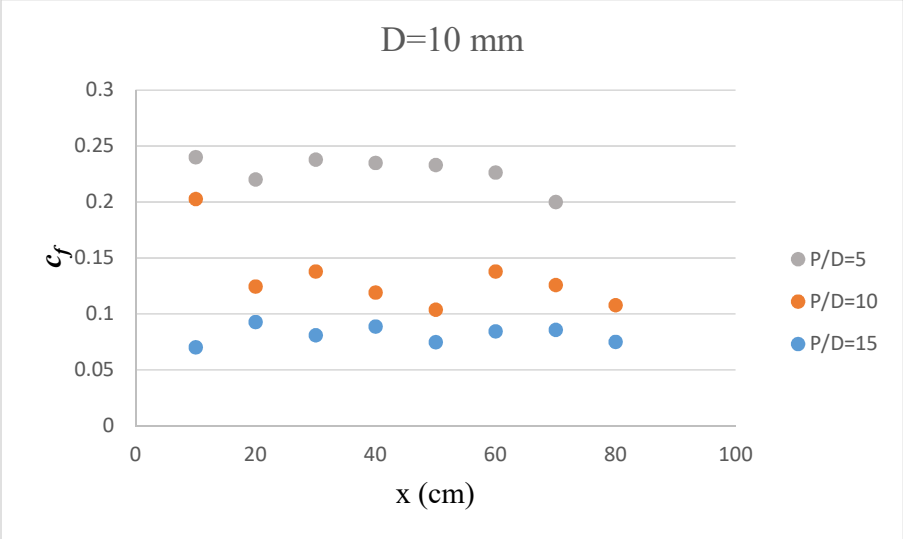

Figure 4-13 - Drag Coefficient Cf Changes in Cylindrical Bed for D = 10 mm and H = 8 cm

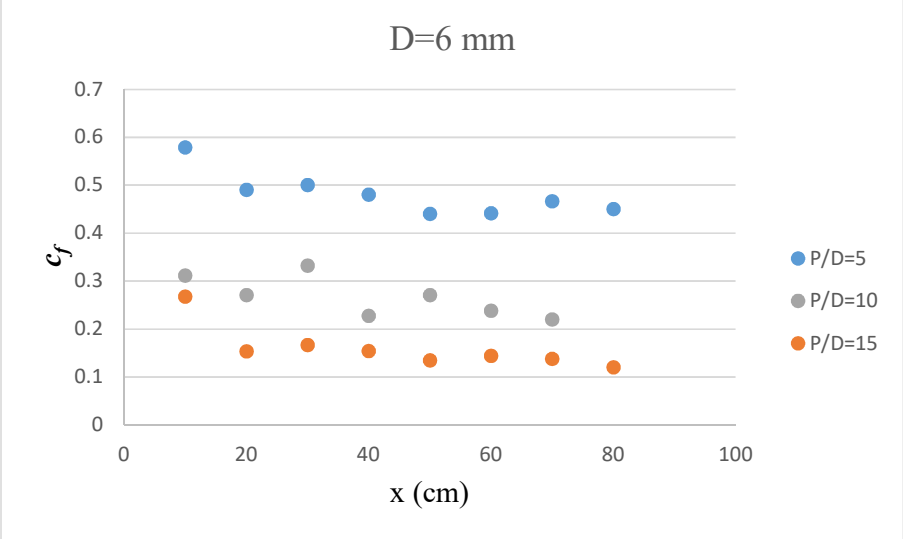

Figure 4-14- Drag coefficient Cf changes along the cylindrical bed for D = 6 mm and H = 6 cm

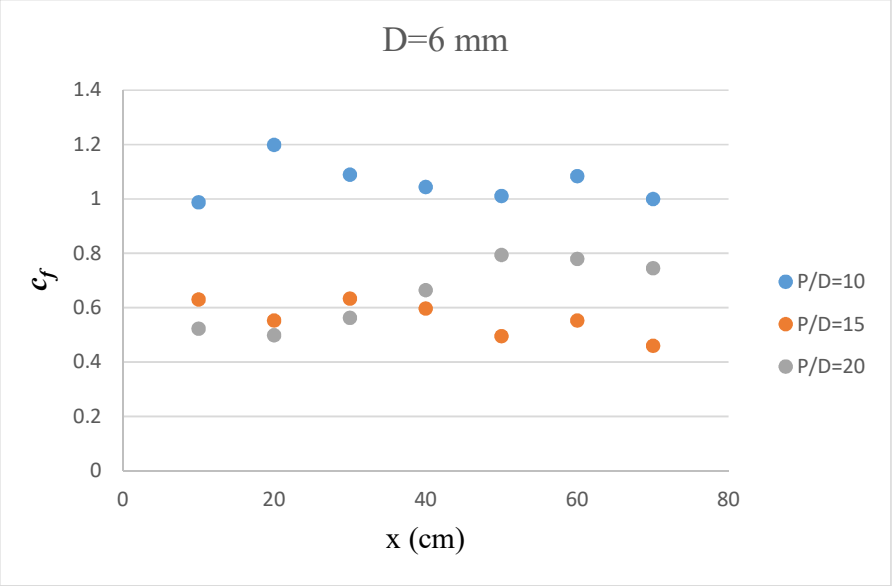

Figure 15-15 - Drag coefficient Cf changes along the cylindrical bed for D = 6 mm and H = 8 cm

Table 4-1. Boundary layer parameters for the test cases

Beds	**P/D**	**H (cm)**	**D (mm)**	**D^+**	**ΔU^+**	**C_f**	**F_T**
Cylindrical (1)	5	8	10	323	14.04	0.104	0.416
	10	8	10	363	12.73	0.072	0.291
	15	8	10	471	11.31	0.05	0.2
	5	6	10	693	8.56	0.49	1.96
	10	6	10	512	11.79	0.23	0.92
	15	6	10	644	10.91	0.137	0.548
Cylindrical (2)	10	8	6	336	9.09	0.278	1.115
	15	8	6	501.6	7.5	0.515	2.061
	20	8	6	506.4	7.75	0.352	1.41
	10	6	6	437.4	8.25	0.373	1.495
	15	6	6	381	7.77	0.371	1.486
	20	6	6	298.2	8.63	0.177	0.711

4-3- Numerical Simulation Model Results

Numerical simulations of the flow on the coarse bed flow profile including water surface profiles, velocity profiles at different cross sections, bed shear stress, flow resistance coefficient and turbulent flow structure on the coarse bed were evaluated.

4.3.1 Calibration and validation of the simulation model

The evaluation of the flow simulation model was performed by calculating the mean relative error statistical index (RAE). The values of this index were determined based on tests performed in laboratory flume and flow simulation with numerical model.

The error was evaluated for the depth and velocity of flow at different sections of the flow. Examination of the simulation error values with the RNG k-ε turbulence model at the calibration and validation stage shows that the relative error for depth and velocity is 1% -15% and is within acceptable range.

4-3-2-Water level profiles

Surface water profiles in the rough bed are determined by RNG k-ε perturbation models. In Figures (4-16) to (21-24) the water surface profiles obtained from the turbulence model are compared with the laboratory data.

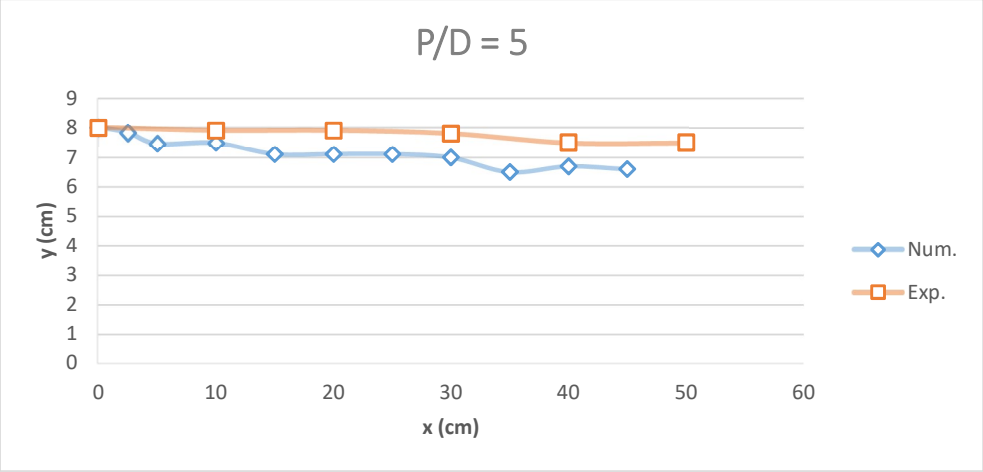

Figure 4-16 - Comparison of water surface profiles obtained from RNG k-ε model and laboratory data on a cylindrical bed for D = 10 mm and H = 8 cm

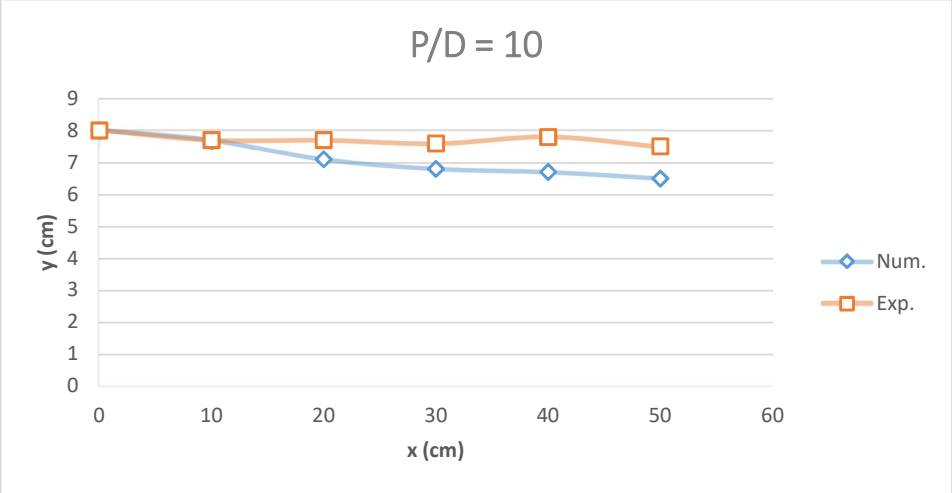

Figure 4-17 - Comparison of water surface profiles obtained from RNG k-ε model and laboratory data on a cylindrical bed for D = 10 mm and H = 8 cm

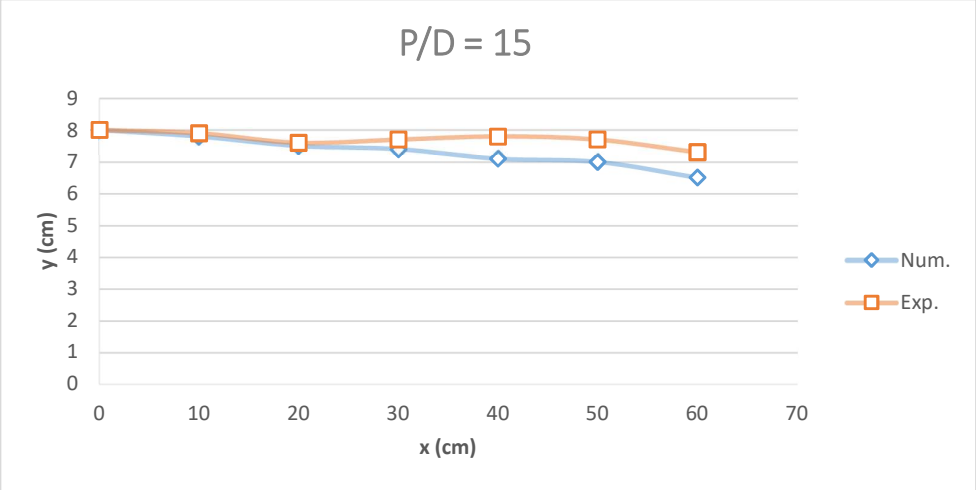

Figure 18-18 - Comparison of water surface profiles obtained from RNG k-ε model and laboratory data on a cylindrical bed for D = 10 mm and H = 8 cm

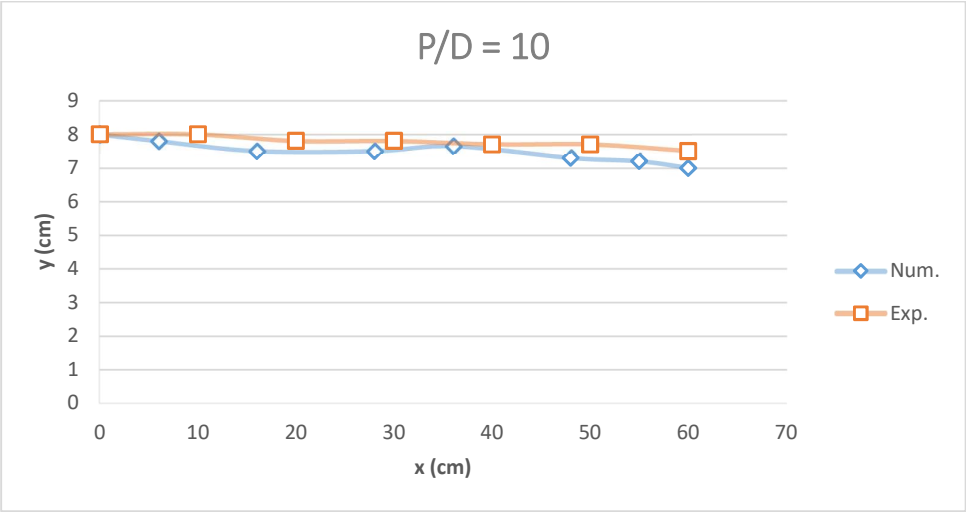

Figure 4-19- Comparison of water surface profiles obtained from RNG k-ε model and laboratory data on a cylindrical bed for D = 6 mm and H = 8 cm

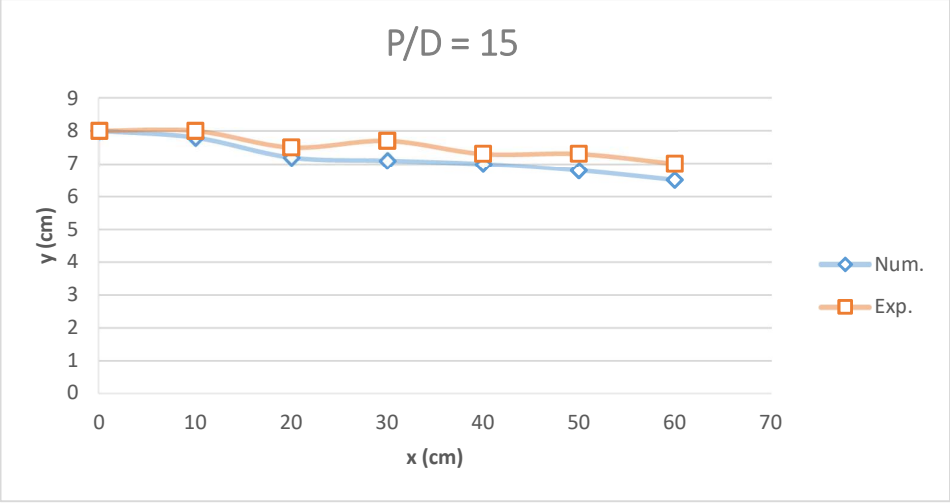

Figure 4-20 - Comparison of water surface profiles obtained from RNG k-ε model and laboratory data on a cylindrical bed for D = 6 mm and H = 8 cm

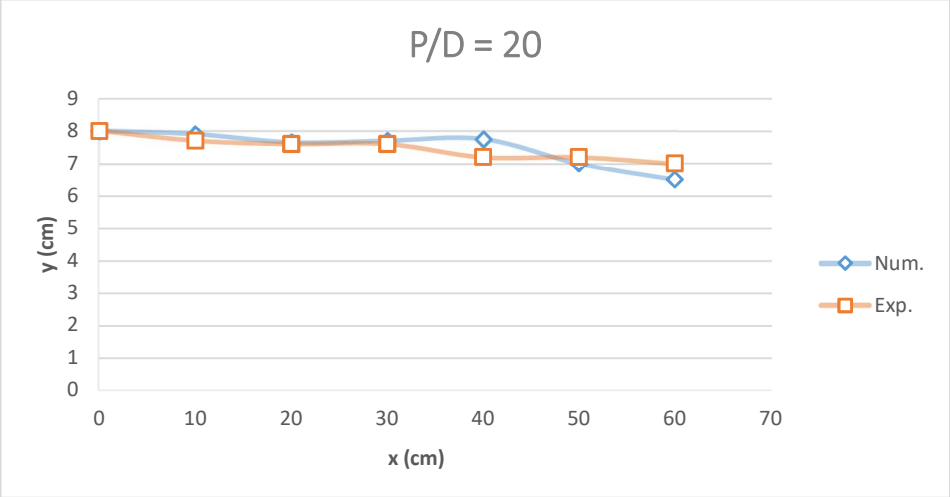

Figure 4-21 - Comparison of water surface profiles obtained from RNG k-ε model and laboratory data on a cylindrical bed for D = 6 mm and H = 8 cm

Figures (21-24) and (22-24) show the free surface water profiles obtained from the RNG k-ε perturbation model using the VOF fluid volume component method for various tests.

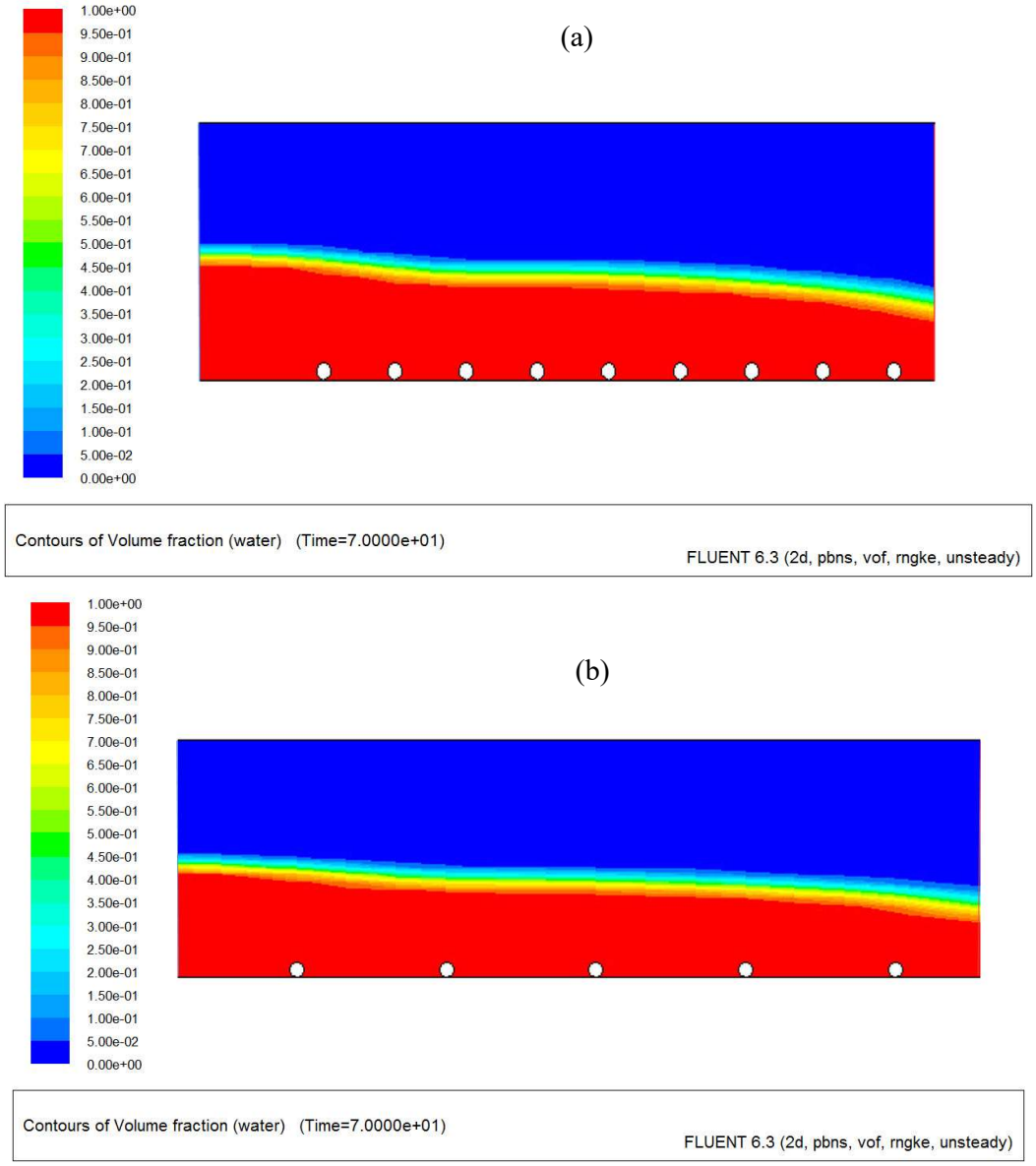

Figure 4-21- Simulation of the free surface profile with RNG k-ε model on the substrate for D = 10 mm a) P / D = 5 and b) P / D = 10

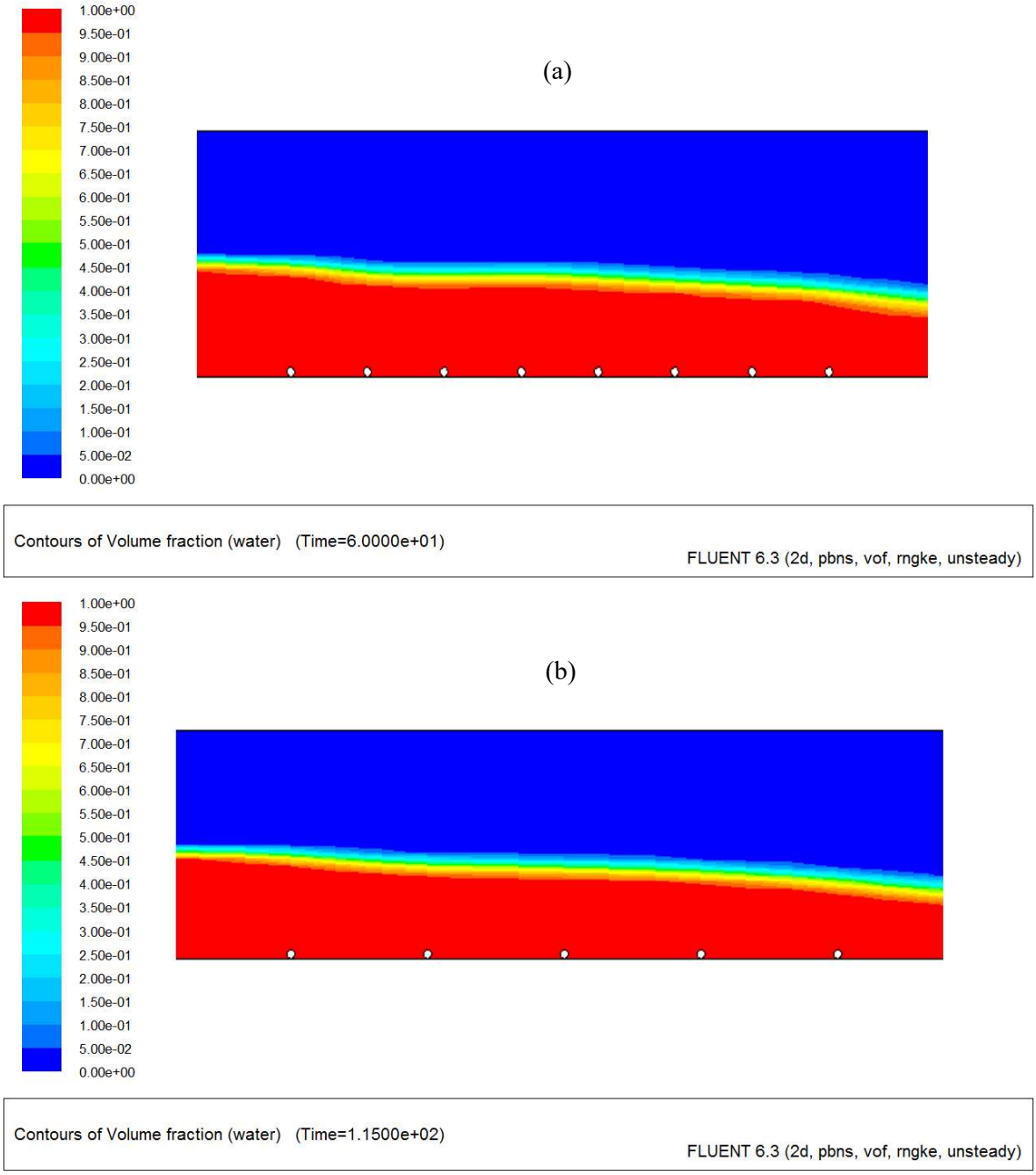

Figure 4-22- Simulation of the free surface profile with RNG k-ε model in cylindrical bed for D = 6 mm a) P / D = 10 and b) P / D = 15

4.3.3 Speed profiles

In Figures (4-23) to (26-24) the velocity profiles obtained from the RNG k-ε perturbation model with and experimental data at different sections of rough substrates are shown.

Given these figures, it can be concluded that the velocity distribution in the various tests is the same and the results obtained from the perturbation models and the laboratory data are in good agreement.

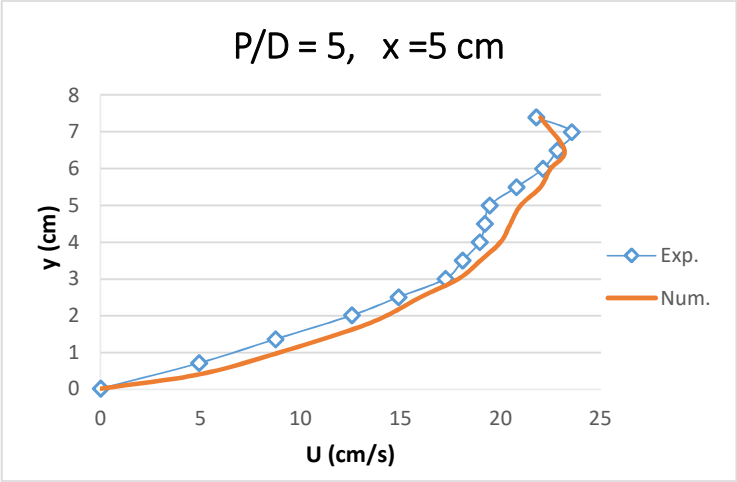

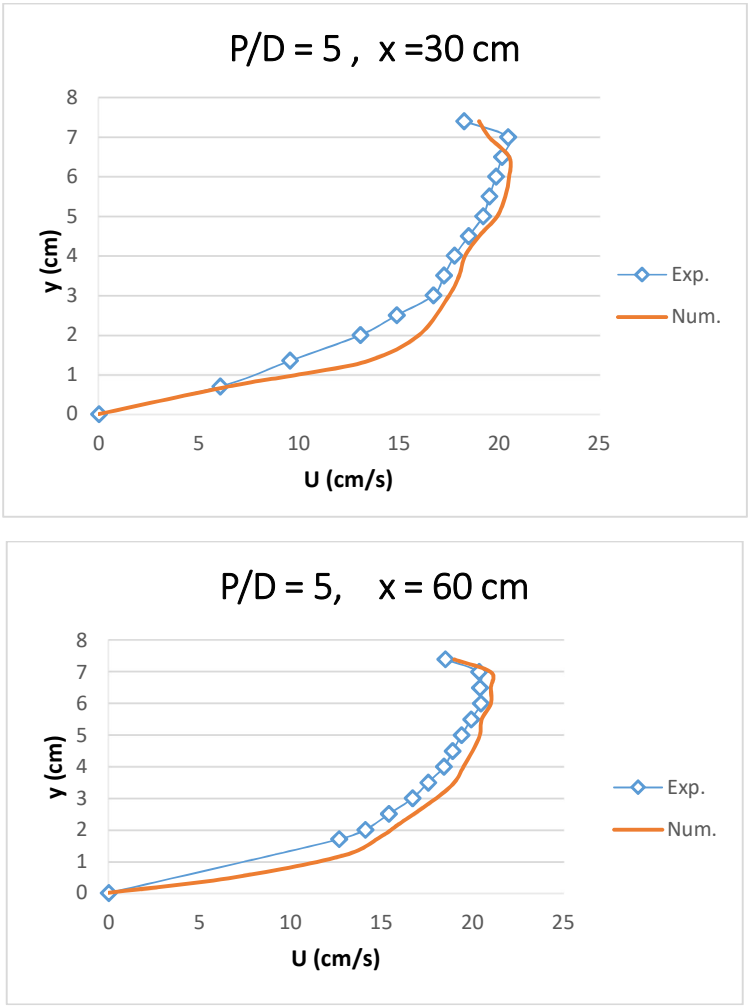

Figure 4-23- Speed profiles obtained from RNG k-ε model on a cylindrical bed for D = 10 mm and H = 8 cm

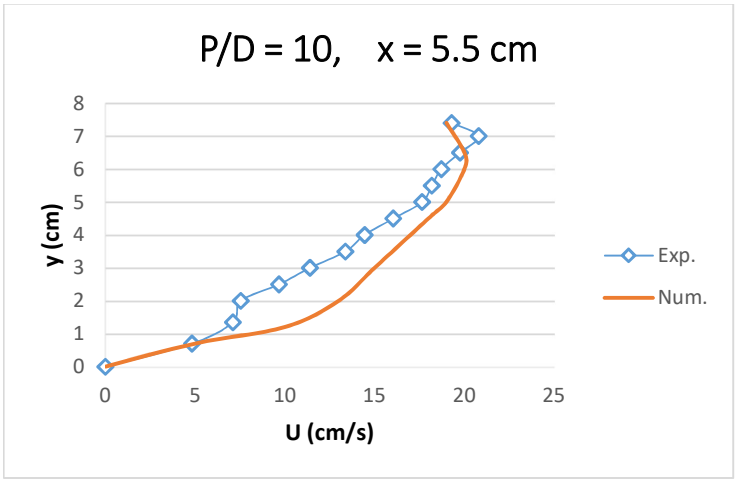

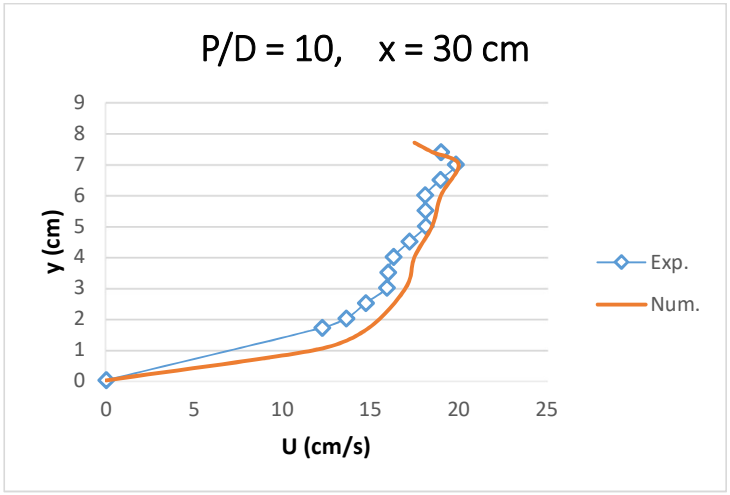

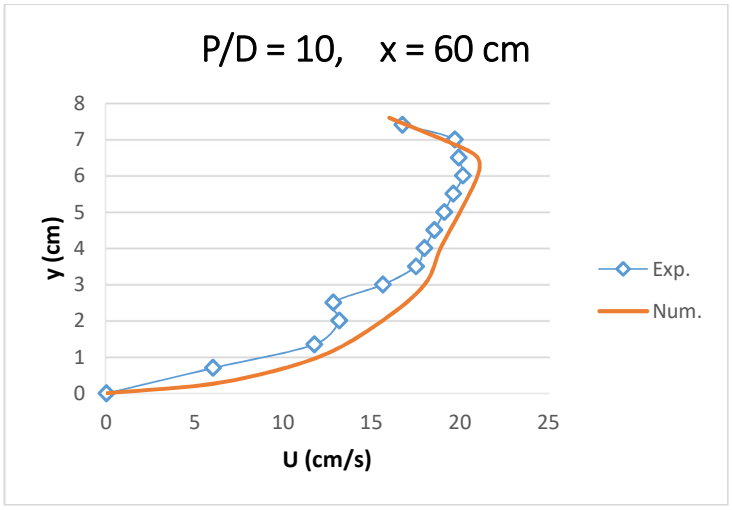

Figure 4-24 - Speed profiles obtained from the RNG k-ε model on a cylindrical bed for D = 10 mm and H = 8 cm

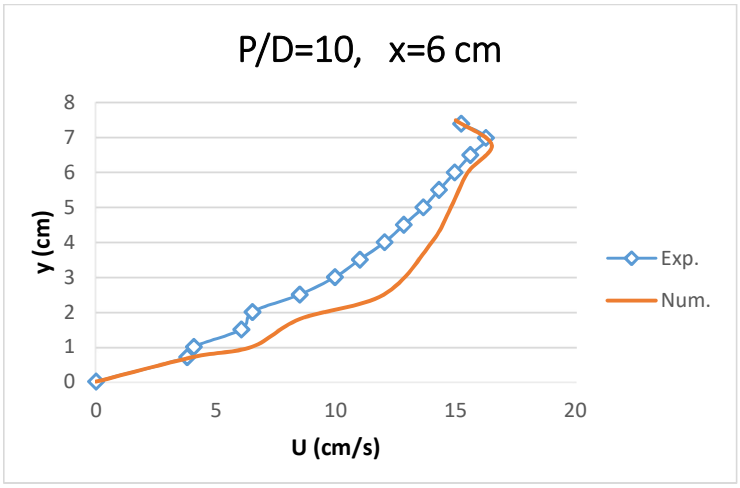

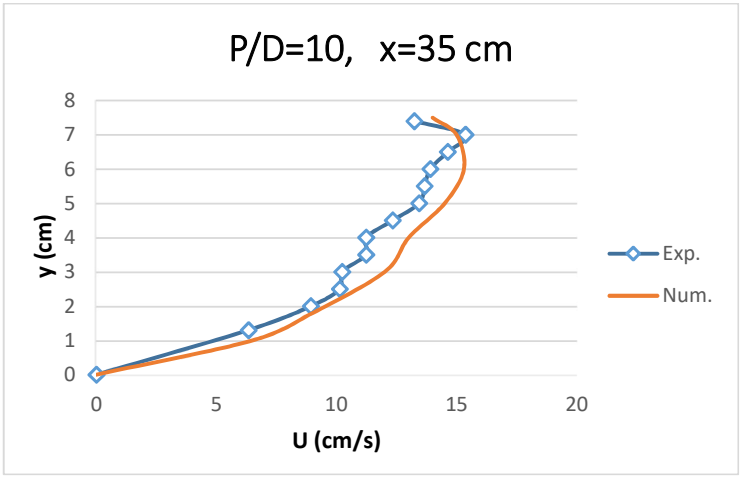

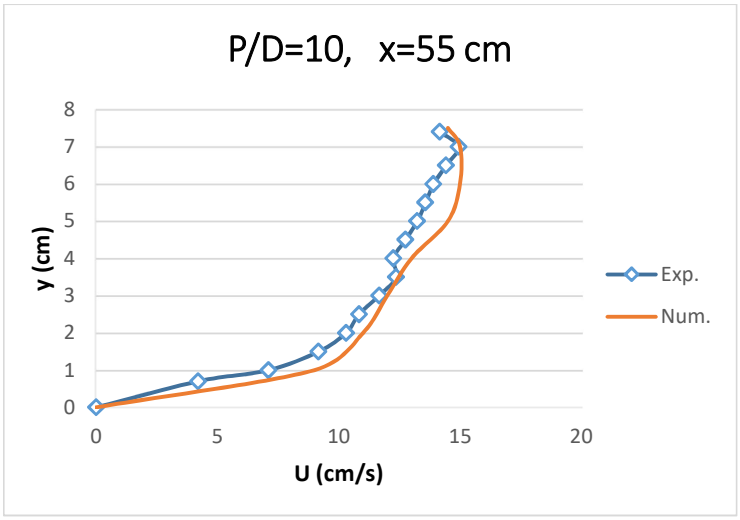

Figure 4-25- Speed profiles obtained from the RNG k-ε model on a cylindrical bed for D = 6 mm and H = 8 cm

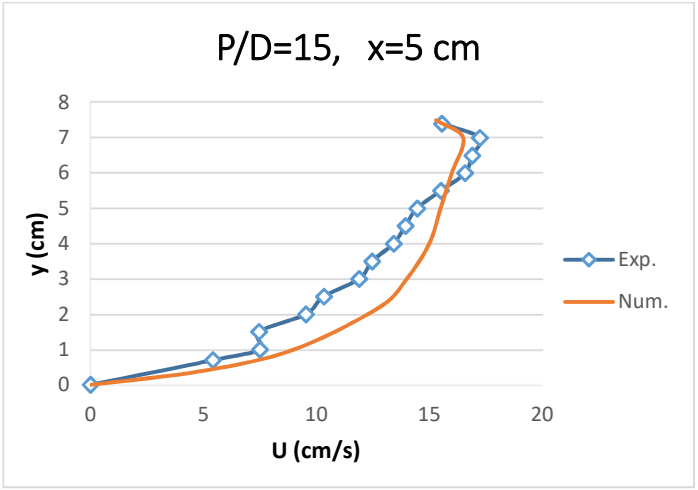

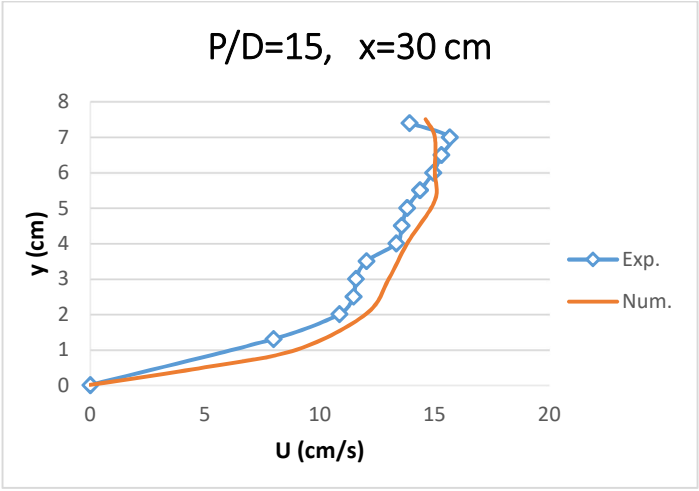

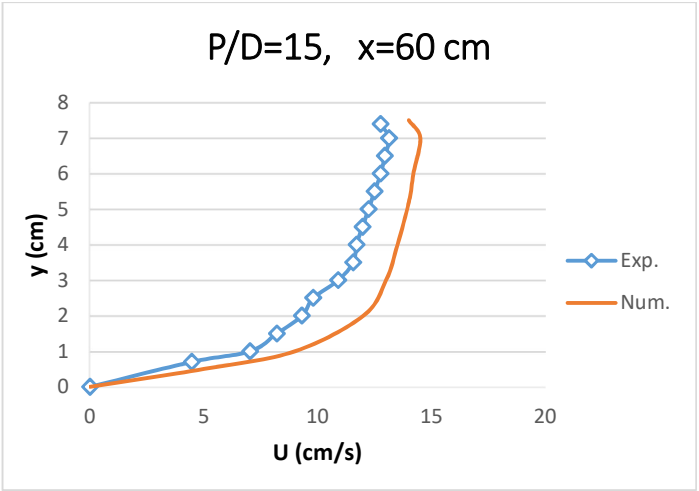

Figure 4-26- Speed profiles obtained from RNG k-ε model on a cylindrical substrate for D = 6 mm and H = 8 cm

Figure (4-27) illustrates the simulated velocity curves simulated by the RNG k-ε perturbation model. From these results, the flow velocity in different regions of the bed can be obtained. The results show that the maximum velocity is at the bottom of the rough bed and the minimum velocity is near the surface of the rough surface. Downstream of the rough bed of gradients, the velocities gradually increase. Zero velocities also occur near the water surface on the rough bed.

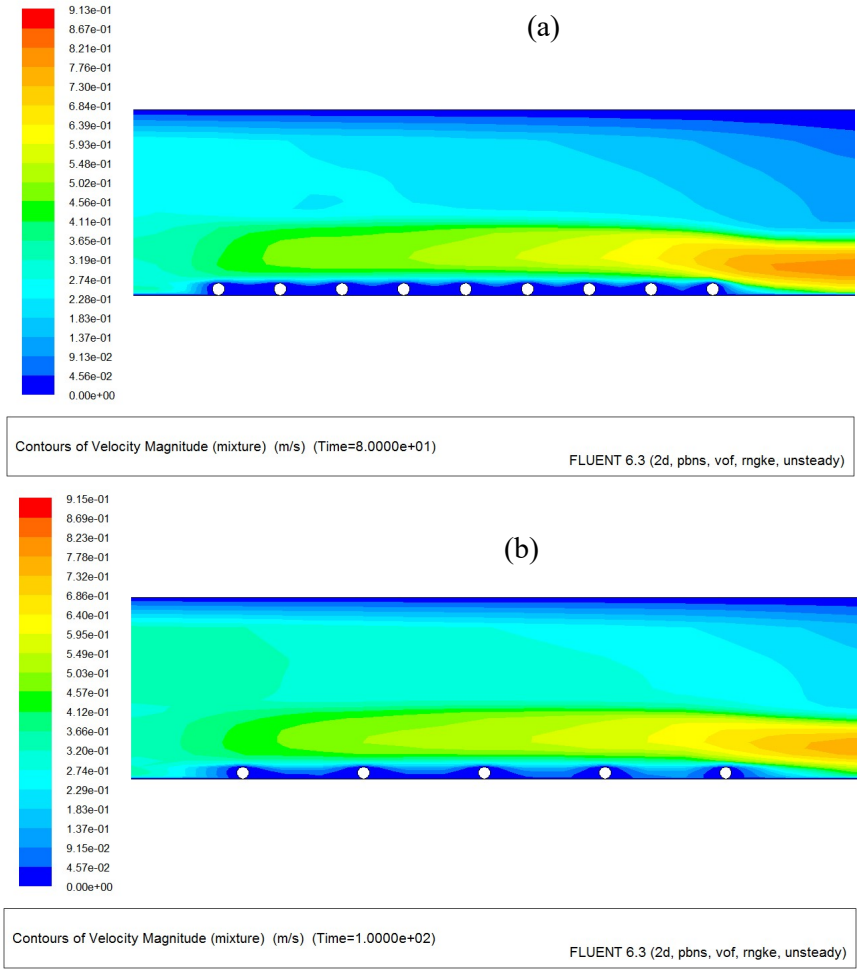

Figure 4-27- Three-dimensional simulation of flow velocity curves in cylindrical bed for D = 10 mm and H = 6 cm a) P / D = 5 and b) P / D = 10

The drag coefficient C_f was determined from (4-4). Figures (4-28) and (29-24) show the drag coefficient of friction C_f obtained from the RNG k-ε model in the rough cylindrical bed. From these figures, it can be concluded that the results of the RNG k-ε model and the experimental results are insignificant.

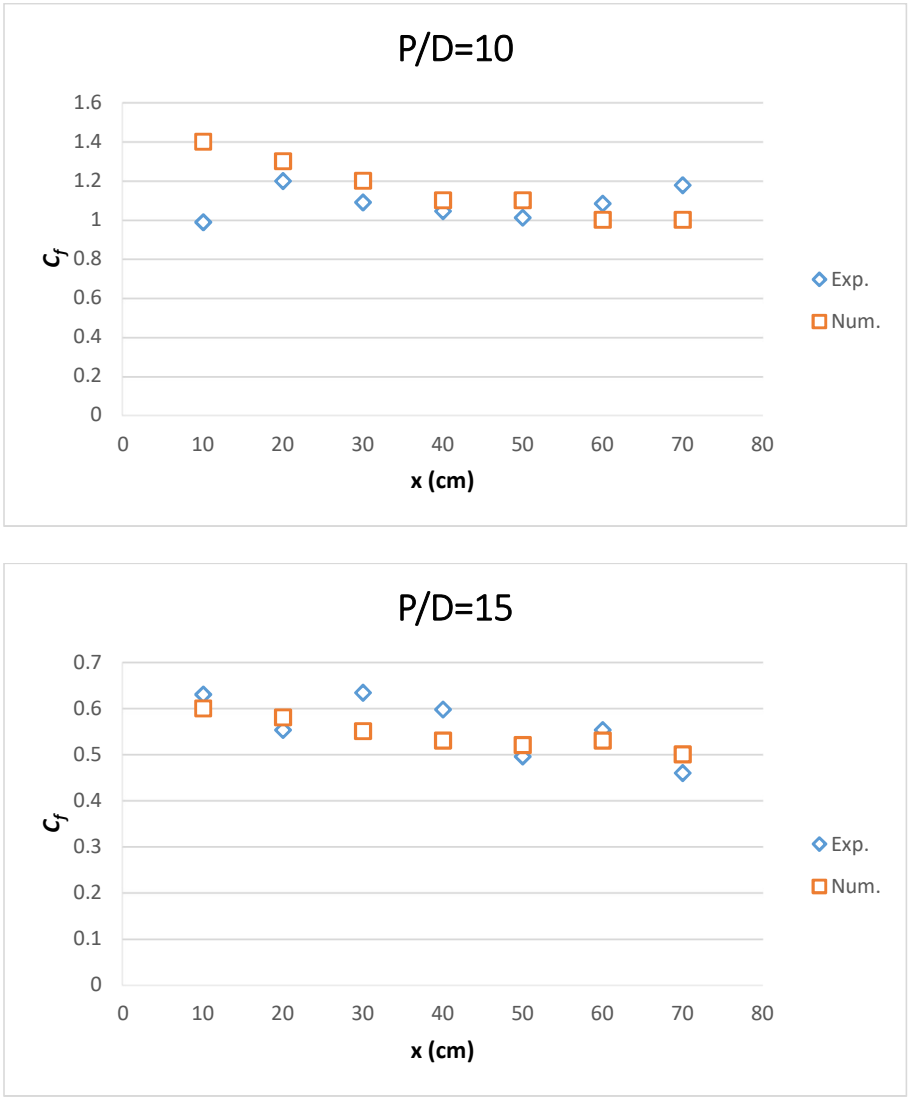

Figure 4-28- Comparison of Cf surface resistance coefficient obtained from RNG k-ε model and laboratory data on cylindrical rough bed for D = 6 mm and H = 8 cm

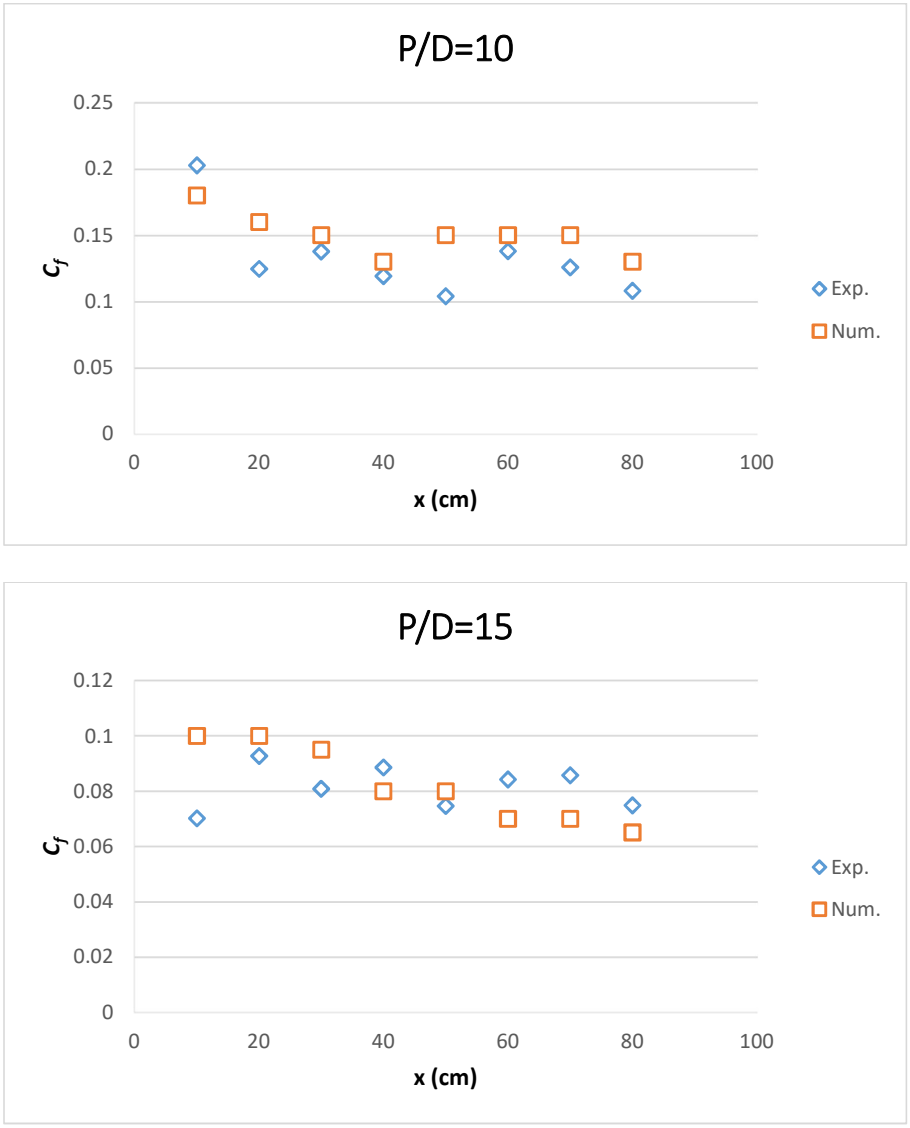

Figure 4-29 - Comparison of surface resistance coefficient Cf obtained from RNG k-ε model and laboratory data on cylindrical rough bed for D = 10 mm and H = 8 cm

3.4- Turbulent flow structure on rough bed

3-4-1-Distribution of turbulence intensities

Figure (4-30) shows the variations of the turbulence intensity. The results show that the turbulence intensities at the bottom of the bed are higher than the upper depths of the bed and the turbulence intensities increase downstream. It can be seen that the maximum turbulence intensities at the end of the cylindrical rough bed (P / D = 10, D = 10 mm) are about 11% (at the bottom of the bed) and the minimum turbulence intensity at the beginning of the rough bed is about 1%. -To be.

Comparison of turbulence intensities in rough substrates shows that turbulence intensity in rough substrates with low roughness intervals is higher than other substrates such that

maximum turbulence intensity in rough substrate substrates with P/D = 5 with D roughness height = 10 mm at the bottom of the rough bed about 12%.

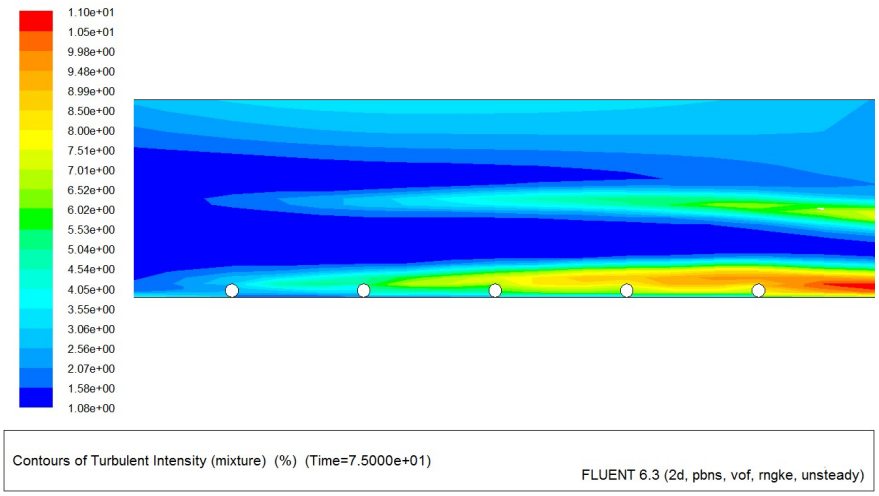

Figure 4-30- Variations of turbulence intensities in the rough cylindrical bed P / D = 10

3-4-2- Distribution of turbulent kinetic energy

Figures (4-31) and (4-32) illustrate the kinetic energy distribution of the turbulence along the rough cylindrical bed with roughness intervals P/D = 5, 10. It can be seen that with increasing distance x the kinetic energy increases and at the end of the bed there is a sudden increase. The results show that kinetic energy was increased near the rough bed (1.5 cm depth of the floor). These values in the bed with roughness intervals P/D = 5 were 0.014 and for roughness intervals P/D = 10 are 0.012 square meters per second squared. In general, the kinetic energy values in the coarse-grained bed are greater than those in the coarse-grained bed.

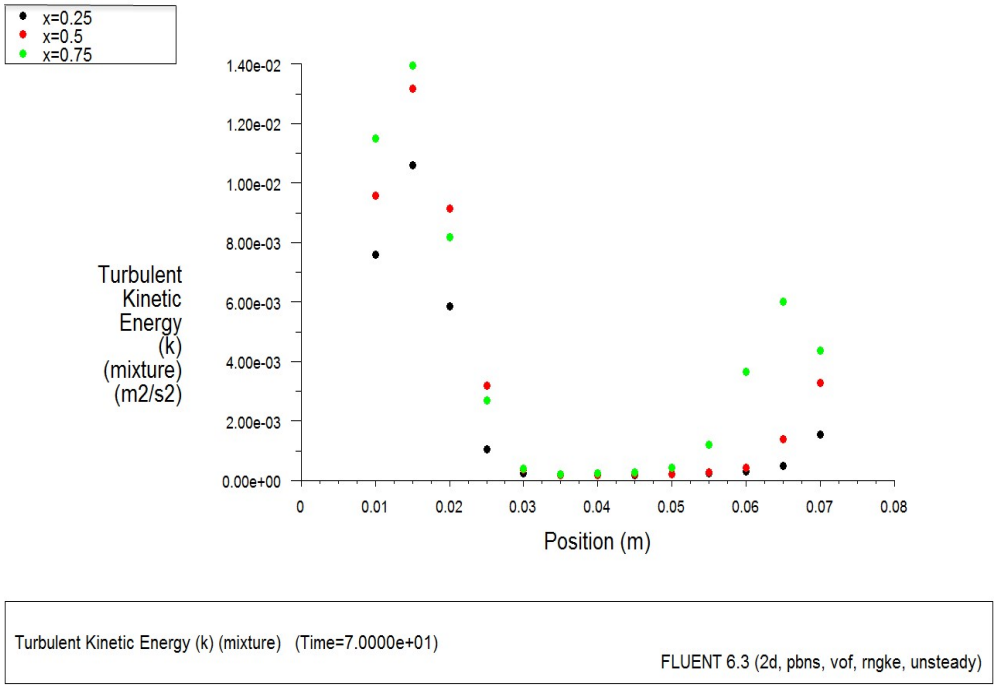

Figure 4-31- Kinetic energy distribution of turbulence along the cylindrical rough bed with roughness intervals P / D = 5

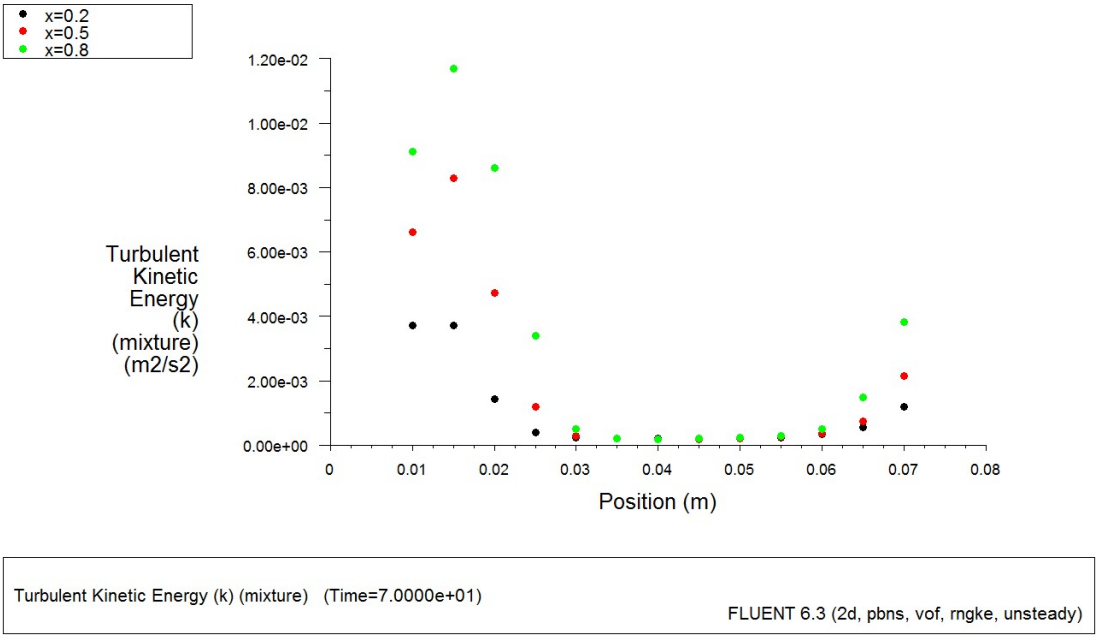

Figure 4-32- Kinetic energy distribution of turbulence along the cylindrical rough bed with roughness intervals P / D = 10

3-4-3-kinetic energy dissipation of turbulence

Figures (4-33) and (4-34) show the kinetic energy dissipation of the turbulence at different distances on the rough bed bottom. It can be seen that the maximum energy loss occurs on the rough bed bumps and increases with increasing distance downstream. Also, by comparing Figures (4-33) and (4-34), it can be concluded that decreasing the roughness distance increases the amount of energy loss. The maximum energy loss is 0.26 m2 / s3. There is also minimal loss of rough bedding to the water surface.

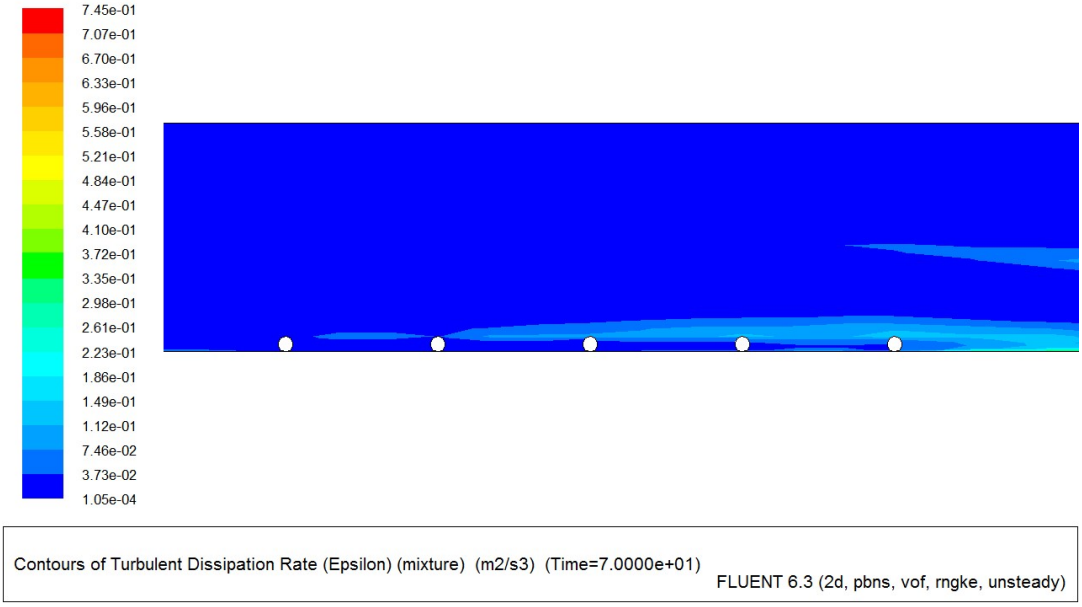

Figure 4-33- Kinetic energy dissipation of turbulence at different distances of cylindrical rough bed for P / D = 10

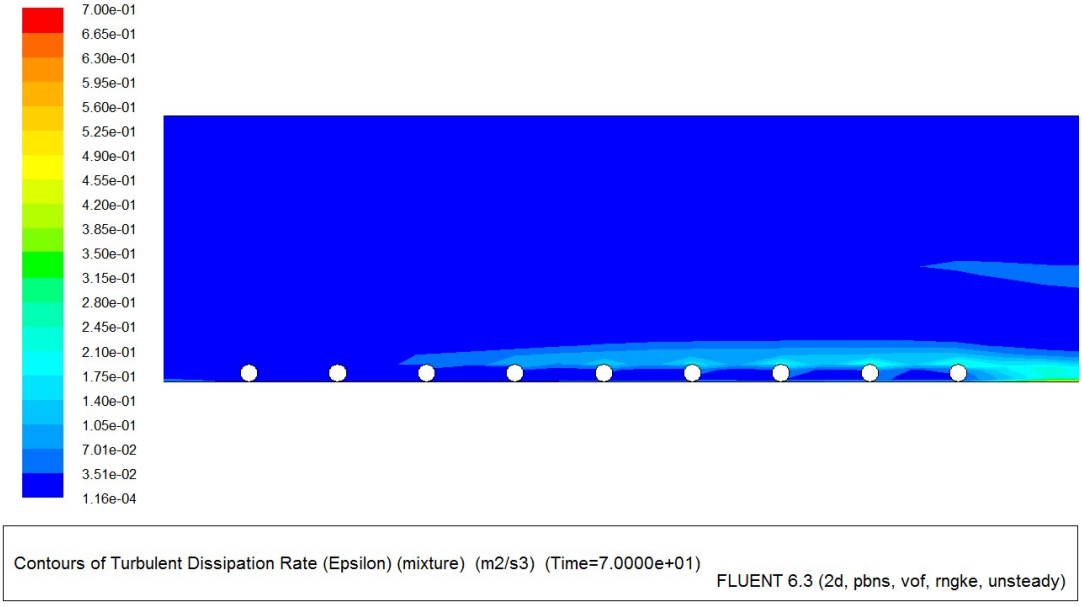

Figure 4-34- Kinetic energy dissipation of turbulence at different distances of cylindrical rough bed for P / D = 5

4-5- Conclusion

4-5-1- Summary of the results of the laboratory examination

In this study, the effect of coarse-grained bed on flow characteristics was investigated. The overall results of the research are presented below.

• Measured data of flow depths at different sections of the channel profile of the water surface. These profiles were used to determine water slope, bed shear stress values, drag coefficient and flow friction.

• The results show that the slope of the water surface in the beds varies with different roughnesses and generally the slope of the water surface decreases with increasing roughness intervals.

• Bed shear stress depends on the slope of the water surface and the hydraulic properties (flow depth and hydraulic radius) of the stream, which decrease with increasing roughness intervals.

• The profiles measured at different flow sections show that the velocity variations in the beds are similar at different roughness intervals. In these profiles, velocity variations are logarithmic so that the velocity increases with increasing distance from the rough bed.

• The velocity profiles at different sections of the rough beds are different from the velocity profiles at the rough surfaces.

• Dimensional velocity profiles of U^+ for dimensionless depth y^+ are plotted for cylindrical roughness. As can be seen in these figures, the dimensional velocities in the rough bed are less than the measured velocities in the flat bed.

The studies show that the average value of the drag coefficient C_f and the friction factor F_t in the rough substrates, decreases with increasing roughness intervals. Also the highest values of drag coefficient and friction factor F_t flow in cylindrical rough bed for D = 6 mm, H = 8 cm and P/D =15 are highest.

4-5-2-Summary of numerical simulation results

In this study, numerical simulation of flow on rough substrates using RNG k-ε turbulence model is presented in the following summary.

• RNG k-ε verification error for different tests shows that RAE values are close and acceptable in estimating water depth and flow rate with the above models.

• RNG k-ε perturbation models and VOF fluid volume component method are suitable for prediction of surface water flow profile on rough bed and are simulated with error of less than 15% of water surface profile. Flow simulation on the rough bed is also considered to be unstable.

• Speed distribution was compared with laboratory data using RNG k-ε perturbation model. The results show that the velocity profiles are similar along the flow and the velocity profiles obtained from the numerical model and the experimental data are consistent.

• Simulated velocity curves simulated by the RNG k-ε turbulence model show that the maximum velocity is at the bottom of the rough bed and the minimum velocity is near the surface of the rough surface. Downstream of the gradient the velocities gradually increase.

• The study of bed shear stress at different flow intervals using RNG k-ε turbulence model shows that with increasing bed roughness intervals the amount of bed shear stress decreases and maximum bed shear stress is almost at the bottom of rough bed Be. Also, the shear stress values on the roughnesses are higher than the stresses on the roughnesses.

• Examination of variations in turbulence intensities at different distances of the coarse bed indicates that the maximum turbulence intensities at the bottom of the bed are about 12% and the minimum turbulence intensity at the beginning of the rough bed is about 1%. Comparison of turbulence intensities in rough substrates shows that turbulence intensities in rough substrates with low roughness intervals are higher than other substrates.

Examination of the kinetic energy of turbulence at different distances of the rough bed indicates that kinetic energy has increased near the rough bed. In general, the kinetic energy values in the coarse-grained bed are higher than those in the coarse-grained bed.

• Investigation of kinetic energy dissipation of turbulence at different distances of the rough bed has shown that the maximum energy loss occurs on the rough bed bumps and increases with increasing downstream distance. There is also minimal energy loss above the rough bed to the water surface.

4-6- Suggestions

• Deformation of roughness and its effect on flow characteristics in open channel.

• Changing the dimensions and spacing of roughness and its effect on flow characteristics in the open channel.

• Comparison of the effect of different roughnesses on the flow in the open channel.

• Investigation of sedimentary flow in open channel with rough bed.

• Experimental 3D study of flow in open channel with rough bed and comparison with numerical models.

• Investigation of flow in open channel with rough bed by other models such as standard k-ε.

References

References

۱. خادمی، مهدی، امید، محمدحسین و هورفر، عبدالحسین. ۱۳۸٤. معرفی نرم افزار دینامیک محاسباتی Fluent. کمیته آبیاری و زهکشی ایران. ۱۵۸ صفحه.

۲. سلطانی، مجید، رحیمی اصل، روح الله. ۱۳۸٦. دینامیک سیالات محاسباتی به کمک نرم افزار Fluent. نشر طراح. تعداد صفحات ٤۳۰.

3. Abbaspour, A., Hashemi Kia, S. (2014). "Numerical investigation of turbulent open channel flow with semi-cylindrical rough beds." KSCE Journal of Civil Engineering, Volume 18, Issue 7, pp. 2252-2260.
4. Abbaspour A and Farsadizadeh D. Study of turbulence structure of open channels with rough bed using physical and numerical modeling. Project No. 2711631-1, Research Affair unit of Tabriz University.
5. Anonymous, 2006. Fluent 6.3 User's Guide. Fluent Incorporated, Lebanon, N.H.
6. Ashrafian, A., Anderssona, H.I. and Manhartb, M. 2004. DNS of turbulent flow in a rod-roughened channel. International Journal of Heat and Fluid Flow, 25, 373–383.

7. Barrantes, A.I. and Madsen, O.S. 2000. Near-bottom flow and flow resistance for currents obliquely incident to two-dimensional roughness elements. J. Geophys. Res., 26, 253-264.
8. Biron, P.M., Robson, C., Lapointe, M.F. and Gaskin, S.H. 2004. Comparing different method of bed shear stress estimates in simple and complex flow field. Earth Surf. Proc. Land. 29 (11), 1403-1415.
9. Bisceglia, S., Smalley, R. J., Djenidi, L. and Antonia R. A. 2001. Structure of rough wall turbulent boundary layers at relatively high Reynolds number, 14th Australasian Fluid Mechanics Conference Adelaide University, Adelaide, Australia, 10-14 December.
10. Bonakdari, H., Larrarte, F., Lassabatere, L. and Joannis, C. 2008. Turbulent velocity profile in fully-developed open channel flows. Environ Fluid Mech , 8, 1–17
11. Coleman, S. E., Nikora, V. I., McLean, S. R., Clunie, T. M., Schlicke, T. and Melville, B. W. 2006. Equilibrium hydrodynamics concept for developing dunes. Phys. Fluids,18(10), 1–12
12. Coleman, S.E, Nikora V.r., Mclean, S.R. and Sclich, E. 2007. Spatially averaged turbulent flow over square ribs. Journal of Engineering Mechanics, 133(2), 194-204.
13. Cui, J., Patel, V.C. and Lin, C-L. 2000. Large-eddy simulation of turbulent flow over rough surfaces. Technical Rep. No. 413, IIHR, The Univ. of Iowa, Iowa City, Iowa.
14. Guo, J. and Julien, P.Y. 2008. Application of the modified log-wake law in open-channels. Journal of Applied Fluid Mechanics, 1(2), 17-23.
15. Jimenez, J. 2004. Turbulent flow over rough walls. Ann Rev Fluid Mech, 36, 173–196.
16. Khan, A.A. and Steffler, P.M. 1996. Physically based hydraulic jump model for depth-averaged computation. Journal of Hydraulic Engineering, ASCE, 122(10), 540-548.
17. Lee, J.H., Lee, S.H., Kim, K. and Sung, H.J. 2009. Structure of the turbulent boundary layer over a rod-roughened wall. Intl J. Heat Fluid Flow 25, 1087–1098.
18. Lee, J.H. Sung H.J. and Krogstad, A.P. 2011. Direct numerical simulation of the turbulent boundary layer over a cube-roughened wall. J. Fluid Mech., 10, 1-35.
19. Leonardi, S. Orlandi, S. P., Smalley, R. J., Djenidi, L., Antonia, R. A. 2003. Direct numerical simulations of turbulent channel flow with transverse square bars on one wall. J. Fluid Mech., 491, 229–238.
20. Luis, G.C.E. 2008. Validation of instantaneous velocities measurements with ADV equipment in turbulent high two phase flows. The Eight Int. Conference on Hydro-Science and Engineering (ICHE). September 8–12, Nagoya, Japan.
21. Nezu, I., Kadota, A. and Nakagawa, H. 1997. Turbulent structure in unsteady depth-varying open channel flows. J. Hydraulic Eng., 123, No.9.

22. Nikora, V., Koll, K., McEwan, I., McLean, S. and Dittrich A. 2004. Velocity distribution in the roughness layer of rough-bed flows. J. Hydraulic Eng., 130, 121-129.
23. Nikora, V. I., McLean, S. R., Coleman, S. E., Pokrajac, D., McEwan, I., Campbell, L., Aberle, J., Clunie, T. M. and Koll, K. 2007a. Double-averaging concept for rough-bed open-channel and overland flows: Applications. J. Hydrol. Eng., 130(5), 443-451.
24. Nikora, V., McEwan, I., McLean, S. Coleman, S.E., Pokrajac, D. and Walters, R. 2007b. Double-averaging concept for rough-bed open-channel and overland flows: Theoretical background, J. Hydraulic Eng. 133(8), 873-883.
25. Nikuradse, J. 1933. Laws of flows in rough pipes, NACA Technical memorandum 1292.
26. Perry, A.E., Schofield, W.H. and Joubert, P.N., 1969. Rough wall turbulent boundary layers. J. Fluid Mech. 37, 383–413.
27. Simpson, R. L. 1973. A generalized correlation of roughness density effects on the turbulent boundary layer. AIAA J., 11, 242–24.
28. Stoesser, T. and Rodi, W. 2004. LES of bar and rod roughened channel flow. Proc., Sixth Int. Conf. on Hydro-Science and Engineering, Brisbane, Australia, National Centre for Computational Hydroscience and Engineering, Univ. of Mississippi, Miss.
29. Stoesser, T. and Nikora V. 2008. Flow structure over square bars at intermediate submergence Large Eddy Simulation study of bar spacing effect. Acta Geophysica, 56, 876-893.
30. Volino, R.J., Schultz, M.P. and Flack, K.A., 2007. Turbulence structure in rough and smooth-wall boundary layers. J. Fluid Mech, 592, 263-293.